8

Evanescent-Wave Pumped and Gain Coupled Whispering-Gallery-Mode Fibre Laser

Xiao-Yun Pu, Yuan-Xian Zhang and Li Feng
Department of Physics, Yunnan University, Kunming, Yunnan, China

1. Introduction

A novel Whispering–Gallery–Mode (WGM) fibre laser is demonstrated by pumping and gain coupling with evanescent-waves in this chapter. The properties of the fibre laser, including energy threshold, produced length and polarization of lasing emission have been investigated. Two important applications of the fibre lasers on optoelectronics, linearly polarized three-color lasing emission and single WGM lasing emission, are also demonstrated in this chapter. The chapter is composed by four parts. In part one, an evanescent wave pumped and gain coupled micro-cavity fiber laser is demonstrated by inserting a bare fused quartz fiber into a glass capillary filled with Rhodamine 6G dye solution, and its energy threshold properties, including the energy threshold varied with the refractive index of the dye solution for different fiber diameters and the produced length of lasing emission, are then investigated. In part two, the polarization properties of an evanescent-wave pumped WGM fibre laser are investigated. It is found that there are two kinds of polarization lasing beam emitting from the evanescent-wave pumped WGM fibre laser under two different pump conditions. In part three, WGM fibre laser, emitting linearly polarized three-color light, is demonstrated by pumping and gain coupling with evanescent waves. In part four, a coupled cylinder-cavity structure, which is used to increase the free spectral range of a WGM fiber laser, is demonstrated by binding two bare optical fibres together, and single WGM lasing emission is realized.

2. Part-I - Threshold property of Whispering-Gallery-Mode fiber lasers pumped by evanescent-waves

In Part I, the threshold properties of Whispering–Gallery–Mode (WGM) fiber lasers pumped by evanescent-waves are investigated. Evanescent-wave gain coupled circular microcavity lasers, such as cylindrical [1-6], spherical[7,8], capillary [9,10] and fiber knot [11] lasers, have generated much interest in recent years, which are due mainly to the fact that the gain media are distributed around their resonators and their potential applications in integrated optics, optoelectronics and optofluidics [12,13] etc. As the evanescent field of a WGM in a circular cavity extends into the gain medium, the gain can be coupled into the WGM that provides optical feedback required by lasing oscillations. To optically excite the gain molecules around a circular cavity, laser beams are usually pumped from the outside of the gain medium [1-5], this pumping configuration, called side-pumping scheme, suffers a low

pump efficiency, because the pump energy is absorbed by all of excited molecules, and only a small number of molecules residing in the WGM evanescent field contributes to the optical gain. To solve this problem, evanescent-wave pumping scheme has been used in circular cavities in recent years, such as bare optical fiber [6], capillary[9], and microfiber knot[11], which reduces lasing threshold from 200 μJ /pulse in the side-pumping scheme[1] to 9.2 μJ /pulse [9] and further to 100 nJ /pulse[11]. Optical gain in the evanescent-wave pumping scheme is produced by evanescent-waves on a fiber surface, the waves are created by a pump light that propagates within the fiber by total internal reflection. Due to a strong spatial overlap between the gain profile and the WGM evanescent field, a high pump efficiency and a long gain distance along the axis of the circular cavity have been achieved [6], which has been successfully used to invent a WGM fiber laser emitting three-wavelength-range lasing beams in a single optical fiber [14].

In the evanescent-wave pumping scheme, laser resonator is surrounded by a dye solution of low refractive index (RI), which acts not only as the gain medium, but also the cladding material for the pumping and circulating light in a microcavity. The penetration depth of pump light into the dye solution determines the gain value, the smaller RI difference between the cavity material and dye solution is, the larger gain is produced by evanescent-wave pumping scheme. Further more, the quality factor (Q value) of a resonator determines the cavity loss, a small RI difference between the cavity material and dye solution means a large cavity loss, which is not benefit to lasing oscillation. Therefore, the threshold property of an evanescent-wave pumped microcavity laser is affected strongly by the RI of cladding solution. However, few works, either the simulations or the experiments, have been reported to explore this important effect of the microcavity laser.

In this part, firstly, the optical gain of a microcavity fiber laser in the evanescent-wave pumping scheme is analyzed by introducing a Gaussian distribution function of pump light, a gain formula is derived. The energy losses related to a circular cavity, including cavity absorption, light scattering and leakage are considered, which leads to a quality-factor equation. Secondly, assuming the derived gain is equal to the energy loss, the energy threshold formula is achieved that is convenient to be compared with our experimental results. Based on the characteristics of frustrated totally internal reflection (FTIR) of pump light traveling along an optical fiber, an attenuated factor is introduced in the threshold energy formula, to achieve the equation for determining the produced length of lasing emission along the axial of the optical fiber. Thirdly, an evanescent-wave pumped and gain coupled WGM fiber laser is fabricated by inserting a bare fused quartz fiber (no cladding) into a glass capillary filled with Rhodamine 6G dye solution, the energy threshold properties of the laser, including the energy threshold varied with the RI of the dye solution for different fiber diameters and the produced length of lasing emission along the fiber axis, have been experimentally investigated. Fourthly, the experimental results are compared with the theoretical calculations, a summary of this work is given. Finally, the analytical formula for resonant line-width of WGM in a circular cavity is derived, which is arranged as the appendix at the end of this chapter.

2.1 Derivation of the energy threshold and the produced length of lasing emission

2.1.1 Optical gain in evanescent-wave pumping scheme

An optical fiber without cladding is immersed in a dye solution, longitudinally pumped by laser light along the fiber axis, pump beams inside the fiber are the meridian beams [15]

which can be drawn in XZ-plane as shown in Fig.I-1. When a pump beam experiences a total internal reflection at the interface of the fiber and the dye solution, its evanescent-wave (E_p) excites dye molecules and produces an optical gain around the fiber surface. Because fiber cross-section is a circular microcavity that supports WGM oscillation, the optical gain produced by the E_p is within the WGM evanescent-wave (E_w), a strong spatial overlap between two evanescent-waves of E_p and E_w leads to a high pump efficiency in the evanescent-wave pumped WGM fiber laser.

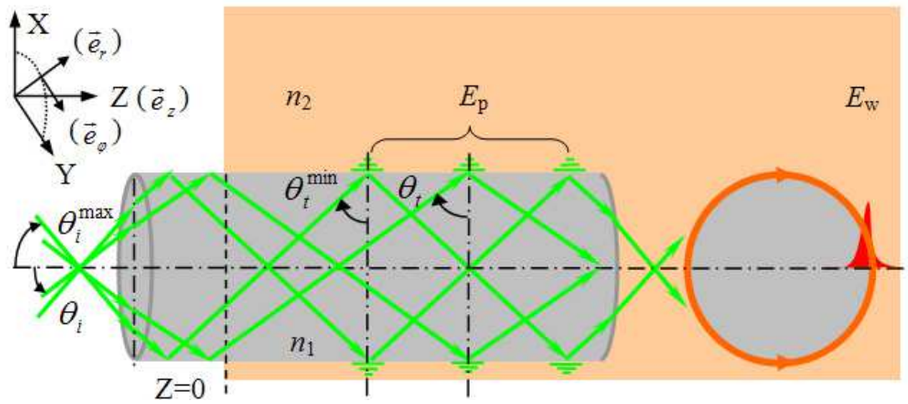

Fig. I-1. The schematic diagram of a WGM fiber laser pumped by an evanescent-wave. Pump light propagating within a bare fiber in the form of meridian beams, θ_i: the entrance angle of a beam on the fiber end face, θ_t: the incidence angle of the beam on the fiber side face, E_P and E_w : the evanescent-fields of a pump light and a WGM.

The evanescence-wave intensity of the pump light can be calculated by [16]

$$I_p(r) = E_p^2(r) = I_0 \exp[-2k(\beta_1 + \beta_2)(r-a)], \ (r \geq a), \tag{I-1}$$

Where a is the fiber radius, $k = 2\pi / \lambda_p$ is the wave vector of the E_p, λ_p is the wavelength of the pump light in vacuum space, $\beta_1 = [n_1^2 \sin^2\theta_t - n_2^2]^{1/2}$ is the attenuated factor induced by total internal reflection, n_1 and n_2 are the RIs of fiber core and cladding solution hereafter ($n_1 > n_2$), θ_t is the incident angle of the pump light on the fiber interface that is larger than the critical angle $\theta_c = \sin^{-1}(n_2 / n_1)$, $\beta_2 = \lambda_p \alpha_{abs}^{p,out}$ is the attenuated factor due to the absorption of E_p by dye molecules, $\alpha_{abs}^{p,out}$ is the absorption coefficient of dye solution at the wavelength λ_p. Assuming the concentration of dye molecules to be N_0, the optical gain coefficient in the small signal condition can be written as

$$g(r) = C(\zeta, \lambda_c, n_2) N_0 \varepsilon_{p0} \exp[-2k(\beta_1 + \beta_2)(r-a)], \ (r \geq a). \tag{I-2}$$

Where pump energy ε_{p0} is used to substitute of the intensity of I_0 for the convenience of comparing the calculation with the experiment, $C(\zeta, \lambda_c, n_2)$ is a coefficient related to coupling efficiency of pump energy (ζ), the fluorescence-quantum efficiency of dye molecules, which is a function of center wavelength of lasing emission (λ_c) and the RI for the clad solution (n_2). After integrating Eq. (2) along radial direction, the total optical gain can be expressed as

$$G = \int_a^{\infty} g(r)dr = \int_0^{\infty} C(\xi, \lambda_c, n_2) N_0 \varepsilon_{p0} \exp[-2k(\beta_1 + \beta_2)R] dR$$

$$= \frac{C(\zeta, \lambda_c, n_2) N_0 \lambda_p \varepsilon_{p0}}{4\pi[(n_1^2 \sin^2\theta_t - n_2^2)^{1/2} + \lambda_p \alpha_{abs}^{p,out}]}. \quad \text{(I-3)}$$

Since the pump-light source is usually a tightly focused laser beams [6, 9, 11], each beam coupled into the fiber incidents upon the fiber side face with different angle θ_t. $\overline{\sin^2\theta_t} = \int_{\theta_t^{\min}}^{\pi/2} f(\theta_t)\sin^2\theta_t d\theta_t$ is used to substitute the term of $\sin^2\theta_t$ in Eq. (3), where the $\theta_t^{\min}$ is the minimum incident angle at fiber side face that relates to the maximum incident angle $\theta_i^{\max}$ at fiber end face as shown in Fig.I-1, $f(\theta_t)$ is the distribution function of incident angle that is defined as the fraction of pump intensity per unit angle. In order to get the $f(\theta_t)$, the intensity distribution of pump light on the fiber end face is assumed to be a Gaussian function, $I(\theta_i) = I_0 \exp[-\tan^2\theta_i / \tan^2\theta_i^{\max}]$. The $f(\theta_t)$ thus can be expressed as

$$f(\theta_t) = f_0 \exp[-\frac{\cos^2\theta_t(1 - n_1^2\cos^2\theta_t^{\min})}{\cos^2\theta_t^{\min}(1 - n_1^2\cos^2\theta_t)}], \quad \text{(I-4)}$$

Where f_0 is the normalized factor that can be calculated by the numeral integration. For the purpose of comparison, a homogeneous distribution function $f(\theta_t) = 1/(\pi/2 - \theta_t^{\min})$ has been used to calculate the term of $\sin^2\theta_t$, the calculated optical gains for both distribution functions are shown in Fig.I-2. Let $\sin^2\theta_t$ be equal to $\sin^2\theta_t^{\max}$, the calculated gain curves are also shown in Fig.I-2.

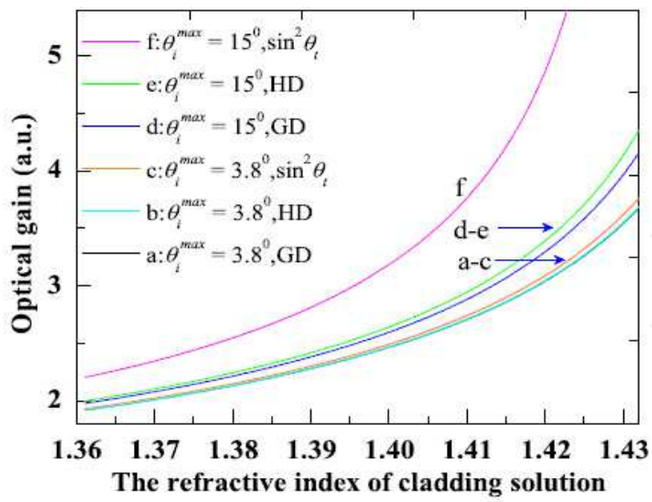

Fig. I-2. The calculated optical gains varied with the RI of cladding solution. The curves a-c: $\theta_i^{\max} = 3.8^\circ$ ($\theta_t^{\min} = 87.4^\circ$), the curves d-f: $\theta_i^{\max} = 15^\circ$ ($\theta_t^{\min} = 79.8^\circ$). HD: homogeneous distribution, GD: Gaussian distribution. In the calculations, n_1=1.458 for the quartz fiber used in our work, λ_p=532 nm, and $\beta_2 = \lambda_p \alpha_{abs}^{p,out}$ = 0.062 for the dye concentration of 4×10^{-3} M/L.

The calculations indicate that (1) the optical gain increases with the increase of n_2 value and the incident angle θ_i, (2) when the incident angle θ_i is small, the effect of distribution function on the optical gain is not obvious, however, the effect can not be neglected with the increase of the incident angle.

2.1.2 The cavity energy losses

Assuming the Q_{abs}, Q_{leak} and Q_{sca} to be the quality factors of a circular cavity related to the energy loss coefficients α_{abs}, α_{leak} and α_{sca}, which are caused by cavity absorption, light leakage and scattering, respectively, the total quality factor (Q_{tol}) of a WGM in a cylindrical cavity can be expressed as

$$\frac{1}{Q_{tol}} = \frac{1}{Q_{abs}} + \frac{1}{Q_{leak}} + \frac{1}{Q_{scat}} \tag{I-5}$$

The absorption loss (α_{abs}) includes the losses inside the cavity ($\alpha_{abs}^{w,in}$, related to the inner field of a WGM) and outside the cavity ($\alpha_{abs}^{w,out}$, related to the evanescent field of a WGM). To calculate it, we assume an occupation factor (η_w) of a WGM in a circular cavity, which is defined as the ratio of the evanescent-field volume to that of the whole WGM [1]. The occupation factor can be written as $\eta_w = \int_a^\infty |E(r)|^2 rdr \Big/ \int_0^\infty |E(r)|^2 rdr$. For a TE wave in a cylindrical coordinate system shown in the top left of Fig.I- 1, the EM field of a WGM in a cylindrical cavity can be written as [17] ,

$$\vec{H}(r) = A_1 J_n(n_1 k_n^l r)\vec{e}_z, \quad (0 \le r \le a), \tag{I-6a}$$

$$\vec{H}(r) = A_2 H_n^{(1)}(n_2 k_n^l r)\vec{e}_z, \quad (r \ge a), \tag{I-6b}$$

$$\vec{E}(r) = D_1\left[\frac{n}{n_1^2 r} J_n(n_1 k_n^l r)\vec{e}_r - \frac{k_n^l}{n_1} J_n^{'}(n_1 k_n^l r)\vec{e}_\phi\right], (0 \le r \le a), \tag{I-6c}$$

$$\vec{E}(r) = D_2\left[\frac{n}{n_2^2 r} H_n^{(1)}(n_2 k_n^l r)\vec{e}_r - \frac{k_n^l}{n_2} H_n^{'(1)}(n_2 k_n^l r)\vec{e}_\phi\right], (r \ge a). \tag{I-6d}$$

Where A_1, A_2, D_1 and D_2 are constants; a is the radius of the cavity; J_n and $H_n^{(1)}$ are the n^{th} Bessel and Hankel functions of the first kind, the derivative of the function denoted by a prime is respect to its argument hereafter; $k_n^l = 2\pi a / \lambda_l^n$ is the wave vector in vacuum for the n^{th} angular mode number and l^{th} radial mode order of a WGM. The occupation factors for (l, n) = (1,745), (1, 1530) and (1, 2256), which correspond to fiber diameters ($2a$ = 93 ± 1μm, 196 ± 1μm and 296 ± 1μm) used in our work and the resonant wavelengths at 576.94, 583.14 and 583.72 nm, have been calculated as the function of n_2 value, the calculated results are shown in Fig.I-3 as the violet dotted lines. The absorption coefficient is $\alpha_{abs} = (1-\eta_w)\alpha_{abs}^{w,in} + \eta_w \alpha_{abs}^{w,out}$, and the quality factor related to the α_{abs} thus can be written as

$$Q_{abs} = (\frac{1}{Q_{abs}^{in}} + \frac{1}{Q_{abs}^{out}})^{-1} = [\frac{\alpha_{abs}^{w,in}\lambda_l^n(1-\eta_w)}{2\pi n_1} + \frac{\alpha_{abs}^{w,out}\lambda_l^n\eta_w}{2\pi n_1}]^{-1}. \quad \text{(I-7)}$$

In the wavelength range of 560 to 580 nm, $\alpha_{abs}^{w,in} = 2\times10^{-4}$ cm^{-1} in our calculation, $\alpha_{abs}^{w,out}$ =20.5 to 2.7 cm^{-1} for the dye concentration of 4×10^{-3} M/L, and 41.0 to 5.4 cm^{-1} for the concentration 8×10^{-3} M/L. The calculated Q_{abs} s varied with n_2 value are shown in Fig.I-3 as the red circular points.

For the TE wave, there are two boundary conditions at surface ($r = a$) of a cylindrical cavity, $A_1 J_n(n_1 k_n^l a) = A_2 H_n^{(1)}(n_2 k_n^l a)$ and $\frac{D_1}{n_1} J_n^{'}(n_1 k_n^l a) = \frac{D_2}{n_2} H_n^{'(1)}(n_2 k_n^l a)$, which can be deduced from Eq. (6). As $A_1 D_2 = A_2 D_1$, the characteristic Eq.(6) for TE wave is written as

$$n_2 \frac{J_n^{'}(n_1 k_n^l a)}{J_n(n_1 k_n^l a)} = n_1 \frac{H_n^{'(1)}(n_2 k_n^l a)}{H_n^{(1)}(n_2 k_n^l a)}. \quad \text{(I-8)}$$

Let $x_{l,n} = 2\pi a / \lambda_l^n$ be the size parameter of a circular cavity of radius a, based on Eq. (8) , the Q_{leak} for a TE wave of a WGM can be calculated with the analytic asymptotic formula [18] shown in Eq. (9).

$$Q_{leak} \cong \frac{\pi}{4}(n_1^2 - n_2^2)x_{l,n}^2 \left|H_n^{(1)}(n_2 x_{l,n})\right|^2 \cdot \left[(\frac{n}{n_1 x_{l,n}})^2 + (\frac{Y_n^{'}(n_2 x_{l,n})}{Y_n(n_2 x_{l,n})})^2\right]. \quad \text{(I-9)}$$

The Q_{leak} s of (l, n) = (1,745), (1, 1530) and (1, 2256), have been calculated as the function of n_2 value, the calculated results are shown in Fig.I- 3 as the green solid lines.

The value of Q_{scat} is of the order of 10^{12} for an ultrahigh-Q microsphere with smooth surface [19]. The Q_{scat} s may be degraded to the order of ~10^8 for the fibers used in our work, which corresponds to a scattering loss α_{scat} ~2×10^{-3} cm^{-1}, and can be neglected by comparing with α_{abs} that is in the range of 2 to 0.2 cm^{-1} within the wavelength range of 560 to 580 nm. Therefore, $1/Q_{tol} \cong 1/Q_{abs} + 1/Q_{leak}$, and the total cavity energy loss is expressed as

$$\alpha_{tol} \cong \frac{2\pi n_1}{\lambda_l^n}\left[\frac{1}{Q_{abs}} + \frac{1}{Q_{leak}}\right]. \quad \text{(I-10)}$$

The Q_{tol} s have been calculated as the function of n_2 value, the calculated results are shown in Fig.I-3 as the blue solid lines.

The calculated results indicate that (1) for the fiber with a larger diameter (Fig.I- 3c, 2a = 296 μm), the Q_{leak} is always much larger than the Q_{abs} , the Q_{tol} is determined mainly by the Q_{abs}, as the result, the cavity loss increases smoothly with the n_2 value; (2) for the fiber with a small diameter (Fig.I- 3a , 2a = 93 μm), as the n_2 value increase, the Q_{tol} is also determined by the Q_{abs} if n_2 is smaller than 1.385, however, the Q_{tol} is determined mainly by the Q_{leak} if n_2 is larger than 1.385, which leads to a sharp increase of the cavity loss; (3) for the fiber with a medium diameter (Fig.I- 3b, 2a = 196 μm), the situation is between the cases (1) and (2).

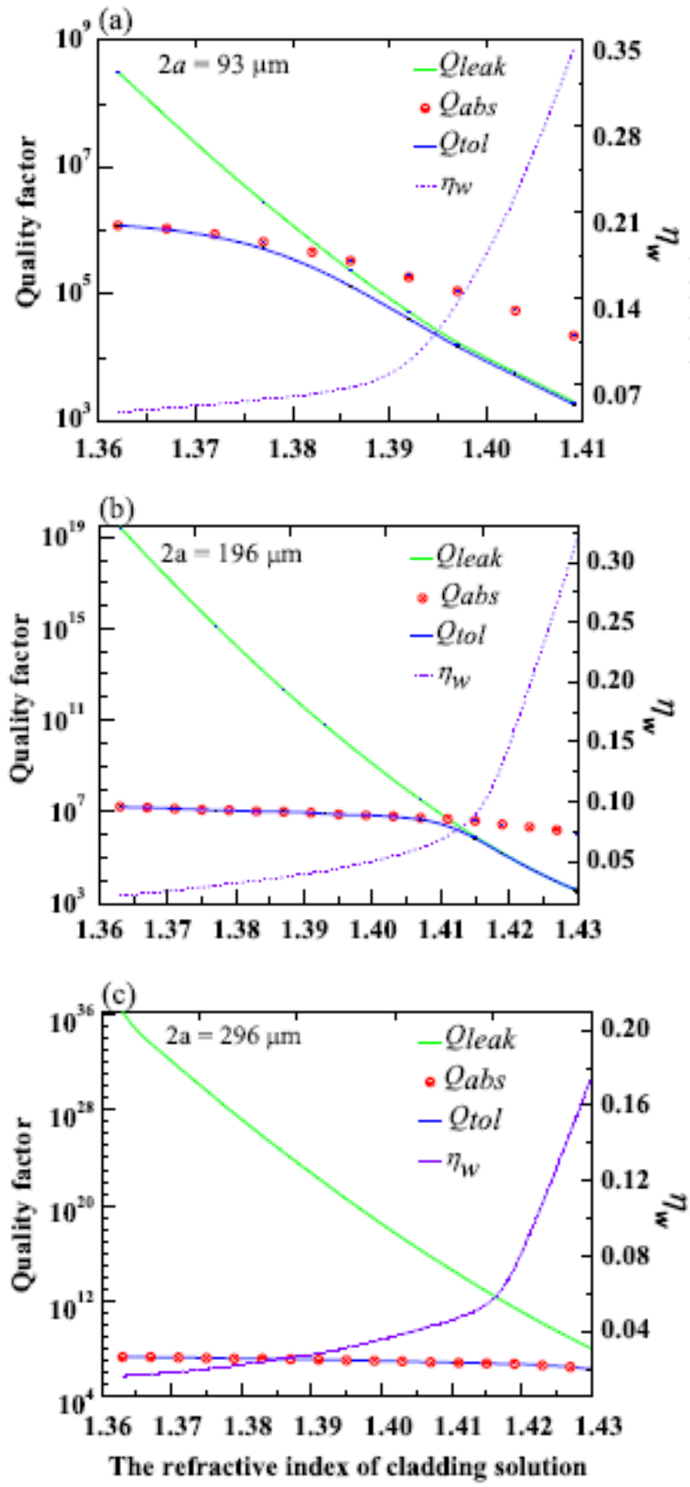

Fig. I-3. Quality factors (Q_{tol} in the blue solid line, Q_{leak} in the green solid line and Q_{abs} in red the circles points) and occupation factor (η_w in the violet dotted line) varied with n_2 value. The calculated fiber diameters are 93 μm in Fig.I-3a, 196 μm in Fig.I-3b and 296 μm in Fig.I-3c.

2.1.3 The formulas of energy threshold and produced length of lasing emission

The threshold condition of lasing action is the gain equaling to the loss. Let Eq. (3) be equal to Eq. (10), the threshold energy can be expressed as

$$\varepsilon_{p0}^{th} = \frac{4\pi[(n_1^2\overline{\sin^2\theta_t} - n_2^2)^{1/2} + \lambda_p\alpha_{abs}^{p,out}]}{C(\zeta,\lambda_c,n_2)N_0\lambda_p}\alpha_{tol}$$

$$= \frac{C^{'}(\zeta,\lambda_c,n_2)[(n_1^2\overline{\sin^2\theta_t} - n_2^2)^{1/2} + \lambda_p\alpha_{abs}^{p,out}][Q_{abs}+Q_{leak}]}{N_0\lambda_p\lambda_l^n Q_{abs}Q_{leak}} \quad \text{(I-11)}$$

Due to the cladding solution is an absorption medium, the pump energy is gradually attenuated along the fiber axis (Z-axis). The energy attenuation is consistent with Beer's law, $\varepsilon_p(Z) = \varepsilon_{p0}\exp(-\alpha_{abs}^p Z)$, where α_{abs}^p is the absorption coefficient of pump light that consists of two parts, the fiber absorption ($\alpha_{abs}^{p,in}$) and the cladding's absorption ($\alpha_{abs}^{p,out}$). Therefore, the optical gain in Eq. (3) must be written as $G(Z) = G(0)\exp(-\alpha_{abs}^p Z)$ at the Z point. To calculate the α_{abs}^p value, similar to the definition of the α_{abs} for a WGM, we define an occupation factor η_p for the pump light, which is the fraction of the evanescent-field intensity to that of the whole pump light. The α_{abs}^p is then written as $\alpha_{abs}^p = (1-\eta_p)\alpha_{abs}^{p,in} + \eta_p\alpha_{abs}^{p,out}$.

The produced length of lasing emission along the Z-axis increases with the pump energy when the energy is larger than the threshold. For a given pump energy, there is a maximum produced length $Z_{\max}$, which corresponds to the optical gain at $Z = Z_{\max}$ equaling to the cavity loss, that is $G(Z_{\max}) = \alpha_{tol}$. The threshold energy at the position $Z = Z_{\max}$ is thus written as $\varepsilon_{p0}^{th}(Z_{\max}) = \varepsilon_{p0}^{th}(0)\exp(\alpha_{abs}^p Z_{\max})$, and the produced length of lasing emission along the fiber axis can be expressed by the logarithmic function as

$$Z_{\max} = \frac{\ln[\varepsilon_{p0}^{th}(Z_{\max})] - \ln[\varepsilon_{p0}^{th}(0)]}{(1-\eta_p)\alpha_{abs}^{p,in} + \eta_p\alpha_{abs}^{p,out}}. \quad \text{(I-12)}$$

Eqs. (11, 12) will be used to compare with the experimental results in Section 2.2.3 of this part.

2.2 Experimental results and discussion

2.2.1 Experimental setup

The experimental setup is shown in Fig.I-4 schematically. The laser beams (532.0 nm), generated by a frequency doubled and Q-switched Nd:YAG laser, was used as a pump light. The required pump energy was obtained by changing the polarization direction of a polarizer (P_1), and its power was monitored by a power meter (PM) through a beam splitter (BS). The polarizer (P_2) was used to determine the polarization state of the pump light. The lenses L_1 and L_2 were used to compress the size of the pump beams. A bare fiber (F_1, RI=1.458) was inserted into a long glass capillary (C, 1 mm in inner diameter, 120 mm in length), the open space between F_1 and C was filled with ethanol and ethylene-glycol mixed solution of the Rhodamine 6G dye with a concentration of 4×10^{-3} M/L. The RI of the mixed solution, acting as the cladding solution, was varied from 1.361 to 1.430 (measured by an

Abbe refractometer) by adjusting the volume ratio of the two solutions. The pump beam was longitudinally coupled into F_1 along the fiber axis by a lens (L_3) (focal length =75 mm) with a conical angle of $2\theta_i$ =7.6°. The beam would propagate within F_1 by FTIR if the entrance angle θ_i was smaller than the critical angle θ_{ic}, which was 15.9° in our experiments. To make sure the pump beams within F_1 were all meridian beams, the incident direction of the pump beams was set to be along the axial direction of F_1.

The WGM lasing emission (L_w) from the rim of F_1 was recorded by a spectrometer (Spectrapro 500i) with an ICCD detector (PI-Max 1024RB) via an optical fiber F_2, which had a 0.05 nm spectral resolution when a grating of density 2400 g/mm was used. The intensity of L_w was detected by a photo detector (PD, DSi200) after the lasing emission passing through an analyzer P_3 positioned on the Y-Z plane, the polarization state of the L_w was checked by rotating P_3. The produced length of the L_w along Z-axis was measured by a ruler, and the fiber sizes were measured by a reading microscopy with an accuracy of 1μm.

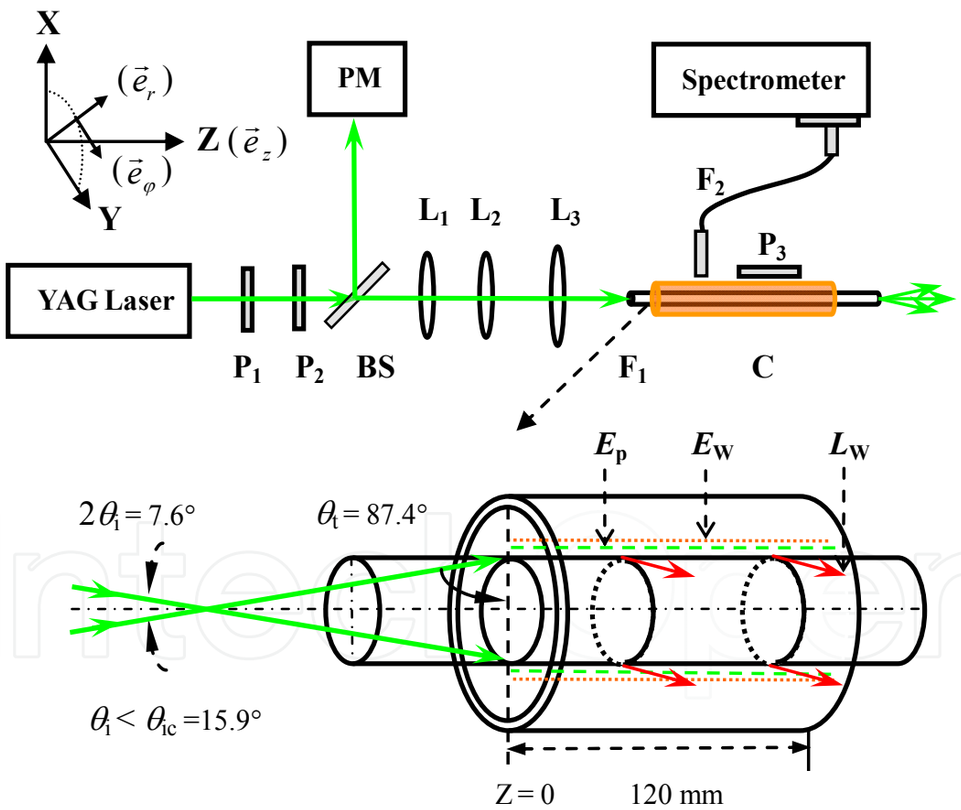

Fig. I-4. Schematic illustration of the experimental set up. P_1, P_2 and P_3: polarizer, BS: beam splitter, PM: Power meter, L_1, L_2 and L_3: lens, F_1: bare quartz fiber, F_2: optical fiber, C: glass capillary, E_P: evanescent field of pump light, E_w: evanescent field of WGM, L_w: WGM laser radiation.

2.2.2 Experimental results

As shown in the insert of Fig.I-5, the output intensities of a WGM fiber laser versus pump energies were measured at the position Z = 0 mm (fiber diameter 196 μm, n_2 = 1.402). When the pump energy was lower than 12.8 μJ/pulse, only a weak spontaneous fluorescence was observed around F_1, once the pump energy was higher than 12.8 μJ/pulse, a strong deep-yellow light emitting from the rim of F_1 was observed in the direction vertical to the F_1's axis (X-Y plane), the energy (12.8 μJ) was the lasing threshold corresponding to the onset of the deep-yellow light. The intensity of lasing emission was found to reach its maximum (or minimum) when the polarization direction of P_3 are vertical (or parallel) to the F_1's axis, meaning that electrical vectors of the lasing emission are perpendicular to the fiber axis, and the evanescent-wave pumped WGM lasing emission is a typical TE wave. When the pump energy was fixed at 100 μJ/pulse, the lasing spectrum recorded by the spectrometer was shown in the Fig. I-5. The interval between any pair of adjacent lasing peaks is about 0.39 nm, slightly larger than 0.38 nm that is calculated by $\Delta\lambda = \lambda^2/2\pi n_1$ (free spectral range). In the calculation of the Q_{tol} in Section 2, the values of λ_l^n and (l, n) should be known in advance. Based on asymptotic formula (Eq. (13)) for the resonant positions of WGMs in cylindrical cavity [20-21], the modes in the lasing spectrum of TE wave in Fig.I-5 were assigned by the pair of numbers (l, n), where a_l is the root of Airy function.

$$\frac{2\pi a_1}{\lambda_n^l} n_1 \approx n + 2^{-1/3} a_l n^{1/3} + \frac{3}{10} 2^{-2/3} a_l^2 n^{-1/3} + 0^{-2/3} . \tag{I-13}$$

For the fiber of diameter 196 μm and the resonant wavelength λ_l^n =583.14 nm, l and n have been assigned by (1, 1525) as indicated in Fig.I-5. Using the same method, for the fibers of diameter 93 μm (λ_l^n =576.94 nm) and 296 μm (λ_l^n =583.72 nm), l and n have been assigned by (1, 745) and (1, 2256), respectively.

The threshold energies varied with the n_2 value were measured for three fibers with different diameters at the position Z = 0 mm, and the results were shown in Fig.I-6. For the fiber of diameter 296 μm, as shown in Fig.I- 6 in green square points, threshold energies decrease monotonously with the increase of n_2 value, which is 25.0 μJ (the maximum) if n_2 = 1.361, and 13.4 μJ (the minimum) if n_2 = 1.430. For the fiber of diameter 93 μm, as shown in Fig.I-6 in the blue triangle points, threshold energies are not sensitive to the change of the cladding solutions when n_2 value is between 1.361 and 1.385, but increase sharply when n_2 value is larger than 1.385. For the fiber of diameter 196 μm, as shown in Fig.I-6 in the red circle points, the threshold energies decrease slowly with the increase of n_2 value when n_2 is between 1.361 and 1.410, beyond the value 1.410, the threshold energies increase sharply and there is minimum threshold value (12.0 μJ) when n_2 = 1.412.

The output intensities versus pump energies at the positions Z = 50 and 80 mm were measured as shown in Fig.I-7 (cladding solution is the same as that in Fig.I-5). The threshold energy is 100.0 μJ/pulse at Z = 50 mm (Fig.I-7a), while it is 190.0 μJ/pulse (Fig.I- 7b) at Z = 80 mm, both values are much larger than 12.8 μJ/pulse measured at Z = 0 mm (Fig.I-5). The results indicate clearly that the threshold energy increases with the measured position (Z), which yields two important issues: first, what experimental law does the pump energy and produced length of lasing emission along the fiber axis follow? Second, which factors affect the produced length of lasing emission?

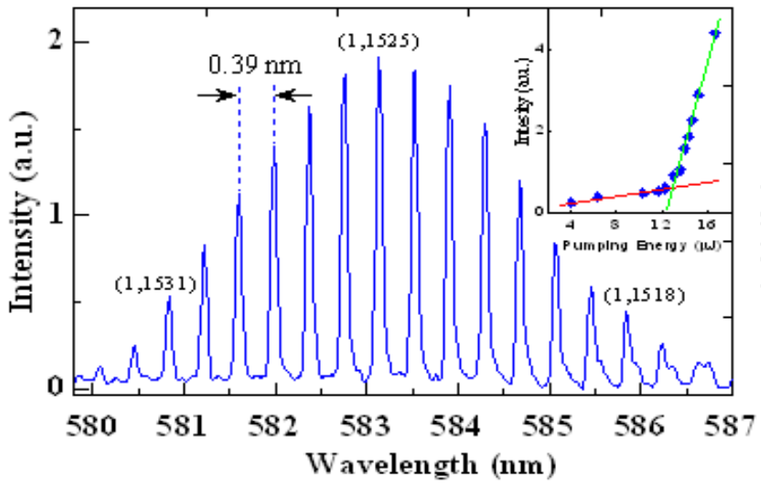

Fig. I-5. Lasing spectrum from the WGM fiber laser of a fiber diameter 196 μm. The output intensities of the laser versus pump energies are shown in the insert of the figure. The measured free spectral range is 0.39 nm indicated by a pair of arrows, and the assigned modes for each lasing peaks are indicated by brackets.

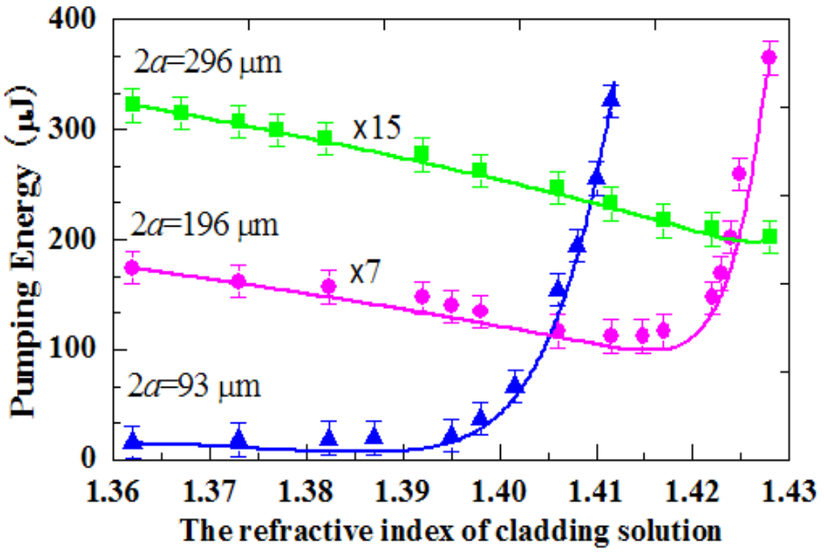

Fig. I-6. Threshold energies varied with the refractive index of cladding solution at the position of Z = 0 mm. Green square points: experimental data for the fiber of diameter 296 μm, red circle points: experimental data for the fiber of diameter 196 μm, blue triangle points: experimental data for the fiber of diameter 93 μm. Solid curves: theoretically calculated results.

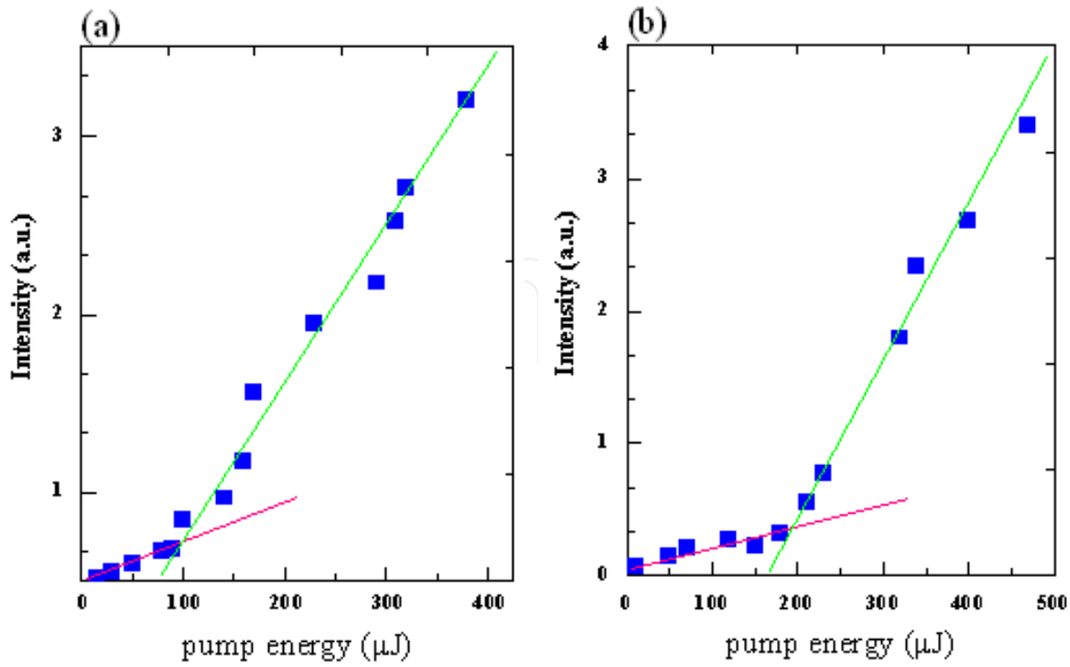

Fig. I-7. The output intensities of a fiber laser versus pump energies at different fiber position (Z). Z = 50 mm in Fig.I-7*a*, and Z = 80 mm in Fig.I-7*b*.

To address the problems mentioned above, a contrastive experiment was carried out by using the fiber of diameter 196 μm. First, different dye concentrations were used with a fixed RI of cladding solution (ethanol, n_2=1.361), and the produced lengths versus the pump energies was measured as shown in Fig.I-8a (c = 4×10^{-3} M/L) and Fig.I-8b (c = 8×10^{-3} M/L). Second, the dye concentration is the same as that in Fig.I- 8a, but the n_2 value is increased to 1.402, the produced lengths versus the pump energies was measured as shown in Fig.I-8c.
The experimental data (red triangle points) in Fig.I-8 shows that the produced length increases dramatically when the pump energy is just larger than the threshold energy at Z = 0 mm, however, the increasing trend become slow when the produced length reaches a certain value, beyond this value, the produced length is almost saturated with the pump energy. Comparing Fig.I-8a with Fig.I-8b, the energy threshold at Z = 0 mm is shifted from 49.0 μJ/pulse in Fig.I-8a (low dye concentration) to 22.0 μJ/pulse in Fig.I-8b (high dye concentration), however, the produced length is decreased from 120 to 89 mm when the pump energy is fixed at 400 μJ/pulse. Comparing Fig.I- 8a with Fig.I-8c, the energy threshold at Z = 0 mm is lowered from 49.0 μJ/pulse in Fig.I-8a (n_2=1.361) to 12.8 μJ/pulse in Fig.I-8c (n_2=1.402), however, the produced length is decreased from 120 to 97 mm when the pump energy is fixed at 400 μJ/pulse. The observed phenomena shown in Fig.I-6 and Fig.I-8 can be well explained by the theory described in Section 2.1.3.

2.2.3 Comparing experimental results with the theoretical calculation

The Eq. (11) is used to calculate the threshold energy varying with n_2 value at the position Z = 0 mm. Each parameter is known except the coefficient $C'(\zeta,\lambda_c,n_2)$ in the Eq. (11). $C'(\zeta,\lambda_c,n_2)$ is treated as $C'(\lambda_c,n_2)$ for a fiber with certain diameter, since the coupling efficiency of pump energy is unchangeable, and $C'(\lambda_c,n_2)$ is approximately treated as

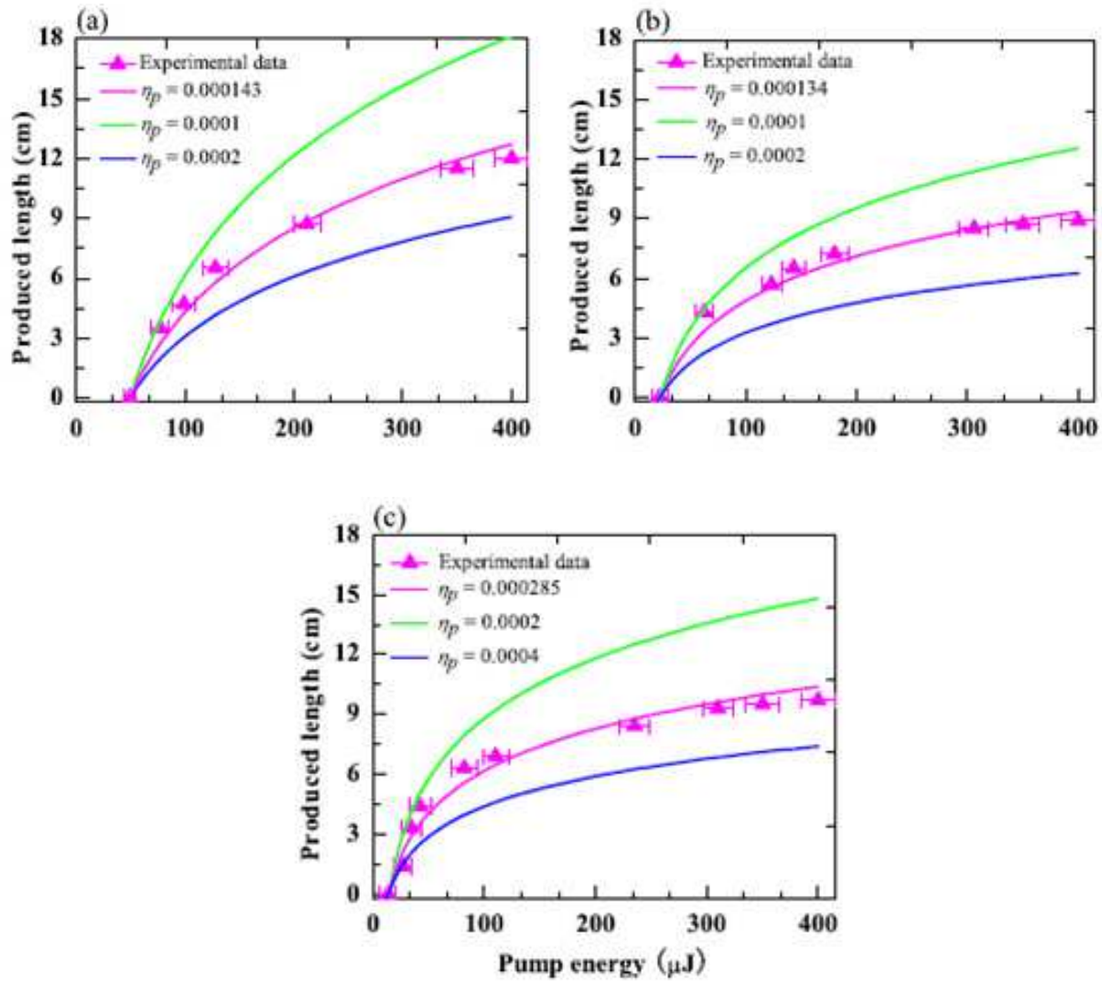

Fig. I-8. The produced length of lasing emission versus pump energy. The n_2 value is fixed at 1.361, but the dye concentrations are 4×10^{-3} M/L in Fig.I- 8a and 8×10^{-3} M/L in Fig.I- 8b. The dye concentration is the same as that in Fig.I- 8a, but the n_2 values is 1.402 in Fig.I- 8c. The red triangle points with error bars are experimental data, the solid curves are theoretically calculated results for various fitting parameters (η_p).

$C'(\lambda_c)$ when solvent effect in dye molecules is negnected. Pairs of experimental data $(n_2, \varepsilon_{p0}^{th})$ and the related Q_{tol} value are substituted into the Eq. (11) to determine $C'(\lambda_c)$. For the fiber of diameter $2a$ = 296 μm at central wavelength λ_c ~583.72 nm, $(n_2, \varepsilon_{p0}^{th}, Q_{tol})$ = (1.361, 21.5μJ, 2.21×10^7), the determined C' =6.07×10^{20}(μJ. m^{-1}). For the fiber of diameter $2a$ =196 μm at central wavelength λ_c ~ 583.14 nm, $(n_2, \varepsilon_{p0}^{th}, Q_{tol})$ = (1.361, 25.0 μJ, 1.66×10^7), the determined C' =5.30×10^{20} (μJ. m^{-1}). For the fiber of diameter $2a$ = 93 μm, three values $(n_2, \varepsilon_{p0}^{th}, Q_{tol})$ = (1.361, 15.5 μJ, 1.19×10^6), (1.386, 20.0 μJ, 1.36×10^5) and (1.409, 256.1 μJ, 1.85×10^3) are chosen to suit the spectral shift with n_2 value, the determined C' (λ_c = 576.94nm) = 2.33×10^{19}, C' (λ_c = 569.91 nm) = 3.86×10^{18} and C' (λ_c = 564.92 nm) = 7.82×10^{17} (μJ. m^{-1}), respectively. The calculated energy thresholds shown in Fig.I- 6 fit the experimental data very well after the C' values are determined.

The dependence of energy threshold on n_2 value for the different fiber diameters can be understood when the properties of optical gain and cavity loss are considered simultaneously. Both optical gain and cavity loss increase with n_2 value, the increment of energy threshold can be expressed by Eq. (11) as

$$\Delta\varepsilon_{p0}^{th}(n_2) = g(n_2)\Delta\alpha_{tol}(n_2) - |\Delta g(n_2)|\alpha_{tol}(n_2), \quad \text{(I-14)}$$

where $g(n_2) = 4\pi[(n_1^2\overline{\sin^2\theta_t} - n_2^2)^{1/2} + \lambda_p\alpha_{abs}^{p,out}]\ /CN_0\lambda_p$ is the factor related to optical gain. If $|\Delta g| / g > \Delta\alpha_{tol} / \alpha_{tol} = |\Delta Q_{tol}| / Q_{tol}$, that is the relative increment of optical gain being larger than that of cavity loss, thus $\Delta\varepsilon_{p0}^{th}(n_2) < 0$, otherwise $\Delta\varepsilon_{p0}^{th}(n_2) > 0$.

For the fiber of diameter 2*a* = 296 μm, $|\Delta g| / g$ is always larger than $\Delta\alpha_{tol} / \alpha_{tol} = |\Delta Q_{tol}| / Q_{tol}$ when n_2 varying from 1.361 to 1.430, thus $\Delta\varepsilon_{p0}^{th}(n_2) < 0$, meaning that the energy threshold decreases monotonously with the increase of n_2, which is shown in Fig.I- 6 as the green square points. For the fiber of diameter 2*a* = 93 μm, $|\Delta g| / g$ is slightly larger than $\Delta\alpha_{tol} / \alpha_{tol}$ when n_2 varying from 1.361 to 1.385, thus $\Delta\varepsilon_{p0}^{th}(n_2) \sim 0$, meaning that the increased optical gain compensates the increased cavity loss and the energy threshold keeps stable; however, $|\Delta g| / g << \Delta\alpha_{tol} / \alpha_{tol}$ after n_2 > 1.385, thus $\Delta\varepsilon_{p0}^{th}(n_2) >> 0$, meaning that more pump energy is required to compensate the cavity loss and the threshold energy increases with the increase of n_2 value, which is shown in Fig.I- 6 as the blue triangle points.

For the fiber of diameter 2*a* = 196 μm, n_2 =1.412 is a critical RI that corresponding to $|\Delta g| / g \sim \Delta\alpha_{tol} / \alpha_{tol}$. When n_2 < 1.412, $|\Delta g| / g > \Delta\alpha_{tol} / \alpha_{tol}$, but $|\Delta g| / g < \Delta\alpha_{tol} / \alpha_{tol}$ when n_2 >1.412. Therefore, there is a minimum threshold energy at n_2 =1.412, which is shown in Fig.I- 6 as the red solid points.

Eq. (12) is used to calculate the produced length of lasing emission varied with pump energy. Fiber absorption coefficient ($\alpha_{abs}^{p,in}$) is 0.0002 cm^{-1}, and the cladding absorption ($\alpha_{abs}^{p,out}$) is 1156 cm^{-1} (2312 cm^{-1}) at λ_p =532 nm for dye concentration of 4×10^{-3} M/L(8×10^{-3} M/L). The occupation factor for pump light (η_p) is still an unknown value that is used as a fitting parameter in Eq. (12), the η_p value for fitting the experimental data best is considered as the true η_p. The fitting results are shown in Fig.I- 8. For the three experimental conditions of (1) *c* = 4×10^{-3} M/L and n_2 = 1.361 in Fig.I- 8a, (2) *c* = 8×10^{-3} M/L and n_2 = 1.361 in Fig.I- 8b, and (3) *c* = 4×10^{-3} M/L and n_2=1.402 in Fig.I- 8c, Eq. (12) fits the experimental data best if η_p = 1.43×10^{-4}, 1.34×10^{-4}, and 2.85×10^{-4}, respectively. It is clear that the experimental data of Z_{max} and $\varepsilon_p^{th}(Z_{max})$ follow Eq. (12) well.

Comparing Fig.I- 8a with Fig.I- 8b in the same n_2 value, a large dye concentration in Fig.I- 8b will attenuate more evanescent field of the pump light, and reduce the penetration depth of the pump light into the cladding solution, leading the η_p value to lower slightly down from 1.43×10^{-4} in Fig.I- 8a to 1.34×10^{-4} in Fig.I- 8b. Based on $\alpha_{abs}^{p} = (1-\eta_p)\alpha_{abs}^{p,in} + \eta_p\alpha_{abs}^{p,out}$, the calculated α_{abs}^{p} values are 0.17 cm^{-1} in Fig.I- 8a and 0.31 cm^{-1} in Fig.I- 8b. A large absorption coefficient α_{abs}^{p}, of cause, will lead to a short produced length of lasing emission for a given pump energy. The energy threshold at the position Z = 0 mm is determined mainly by the dye concentration, the dye concentration in Fig.I- 8b is twice as that in Fig.I- 8a, therefore, the energy threshold at Z = 0 mm is reduced from 49 (*c* = 4×10^{-3} M/L in Fig.I- 8a) to 22 μJ/pulse (*c* = 8×10^{-3}M/L in Fig.I- 8b).

Comparing Fig.I- 8a with Fig.I- 8c in the same dye concentration, a large n_2 value in Fig.I- 8c implies a long penetration depth of the pump light into the cladding solution, which leads η_p value to rise up from 1.43×10^{-4} in Fig.I- 8a to 2.85×10^{-4} in Fig.I- 8c, corresponding α_{abs}^{p} values to increase from 0.17 cm^{-1} to 0.33 cm^{-1}. Based on Eq. (12), the produced length of lasing emission in Fig.I- 8c will be shorter than that of Fig.I- 8a for a given pump energy. The energy threshold at the position Z = 0 mm is determined mainly by n_2 value at this time, a large n_2 value implies a long penetration depth of pump light into cladding solution, and thus a large occupation factor η_p. When η_p value increasing from 1.43×10^{-4} in Fig.I-8a (n_2=1.361) to 2.85×10^{-4} in Fig.I-8c (n_2=1.402), more dye molecules are excited by the given pump energy, it is reasonable that the energy threshold is reduced from 49 to 12.8 μJ/pulse.

3. Part II - Polarization properties of an evanescent-wave pumped Whispering-Gallery-Mode fibre laser

In Part II, the polarization properties of an evanescent-wave pumped Whispering Gallery Mode (WGM) fibre laser evanescent-wave pumping scheme are investigated. The dye gain is produced by the evanescent field of the pump light, therefore, the polarization state of the evanescent field determines the vibration states of excited molecules, consequently the polarization properties of lasing emission of the evanescent-wave pumped WGM fibre laser. We find that when the pump beam is strictly along the axial direction of an optical fibre, the lasing emission is transverse electric (TE) wave and the electrical vector of emitting point is along the radial direction of the optical fibre, which forms a special radial polarized radiation; while the pump beam deviates from the axial direction of the optical fibre, both TE and transverse magnetic (TM) waves exist in the lasing emission, which forms a mixed polarization radiation with radial and axial polarized states. The radial polarization laser is useful in the application of photo-etching [22] and high resolution microscope [23], etc. We report on our experimental results and give the explanation for observed phenomenon in this part.

3.1 Experimental setup

The experiment setup is shown in Fig.II-1. A pulsed Nd:YAG laser (λ=532 nm, pulse width=7 ns) is used as a pump source. The pump laser beams pass two polarizers P_1 and P_2. P_2 is used to determine polarized state of the pump beams, while P_1 is used to change pump energy by rotating its polarization direction. Lenses L_1 and L_2 are used to shrink the pump beams size from original 8 mm to 1.5 mm. F_1 of diameter 196 μm is a barely optical fibre with the refractive index of 1.458. After being focused by lens L_3 (focal length =75 mm), the pump beams are end-fired into F_1 with an incident angle θ_i =1.2°. To make sure the pump light is meridian beams [15] when propagating in F_1, the axis of F_1 is adjusted strictly along the z-axis. The pump light will be skew beams [15] in F_1 when the angle between the axis of F_1 and the z-axis is about 10°.

The fibre F_1 is inserted into a glass tube D with the inner diameter of 2 mm. A mixed solution of ethanol and ethylene glycol doped with Rhodamine 6G dye molecules is filled into the glass tube, and the concentration and refractive index of the dye solution are 3×10^{-3} mol/L and 1.422, respectively. The pump beams will propagate within F_1 by TIR if the incident angle θ_i is smaller than 37.6°. Evanescent field E_p of the pump beams excite the dye

molecules in the dye solution, photons in evanescent field E_{WGM} that belongs to a WGM of circular cavity built in F_1 stimulate the excited molecules, the E_{WGM} also couples dye gain into the circular cavity [1, 2], and then forms lasing oscillation in the circular cavity with the support of the WGM. Lasing energy L_{WGM} radiates from the rim of F_1 in the plane of xy, an optical fibre F_2 transmits part of the L_{WGM} to the entrance slit of the spectrometer (Spectrapro 500i, ICCD：PI－MAX). The intensity of L_{WGM} also can be detected by a photo detector PD (DSi200) after the lasing emission passing the polarizer P_3, which is positioned on the yz plane. The angle between P_3 and the y-axis is defined as Φ which is zero as when P_3 is along in the y-axis direction. Φ can be adjusted by rotating P_3.

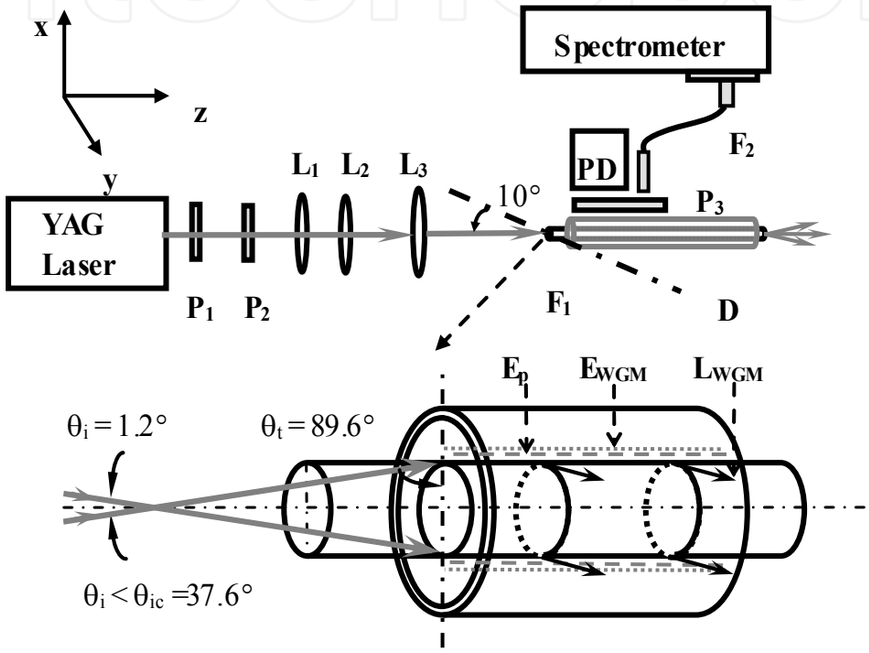

Fig. II-1. Experimental setup

3.2 Experimental results and discussion

3.2.1 Pump along the optical fibre's axis

When pump beams are strictly in the axial direction of F_1, polarizer P_2 is set along the y-axis direction at first. Polarization properties of lasing beams are checked and recorded by PD together with another polarizer P_3, the background subtracted and normalized signals are shown in Fig.II-2. Fig.II-2 shows that the intensity of lasing emission (solid points with error bar) reaches its maximum when P_3 is set vertically to the F_1's axis (Φ=0°,180° and 360°), while it reaches its minimum when P_3 is set along the F_1's axis (Φ=90° and 270°). The curve in Fig.II-2 is drawn by Malu' s Law, $I = \cos^2 \Phi$, the consistency between the curve and experimental data indicates that, when the pump beams are strictly along the F_1's axis, the electrical vector of lasing emission is vertical to the fibre's axis, and the evanescent-wave pumped WGM laser is of a typical TE wave lasing emission. To check the dependence of the lasing emission on the polarization of pump beams, the polarizer P_2 is reset along the x-axis and the middle between x and y-axis, respectively. The experimental results obtained are the same as that when P_2 is set along the y-axis direction, which indicates that the

polarization of evanescent-wave pumped WGM fibre laser is independent on the polarized state of the pump beams.

Removing out the polarizer P_3, the lasing spectrum is recorded with the spectrometer of grating density 2400 g/mm and is shown in Fig.II-3, which shows that the spectrum is consisted of a series of peaks with equal wavelength interval. The mode-assignment results (see text 2.2) also indicate that the spectral lines are the TE wave with the same radial mode order $l=1$ but different angular mode number n[24].

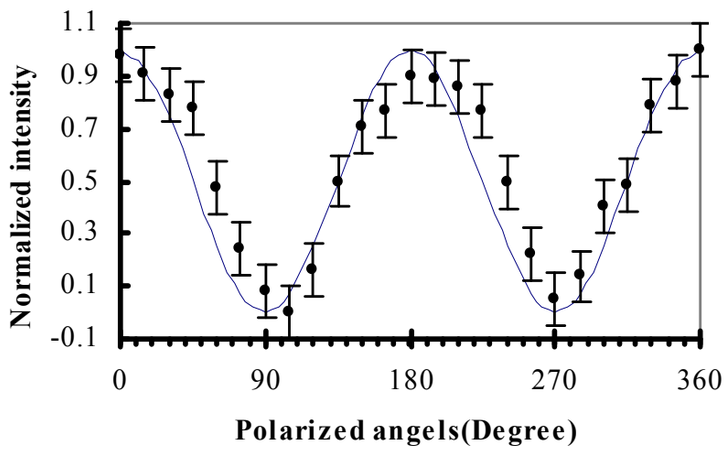

Fig. II-2. The law of WGM laser's intensity varied with polarized angels of polarizer P_3.

3.2.2 The form of radial polarization laser

When pump beams are in the fibre F_1's axial direction, as shown in Fig.II-4-A, the beams are meridian beams that propagate within the fibre by TIR. Hereinafter, the pump beam in xy plane is taken as an example for discussing the polarization properties of the pump beams. When the pump beam travels to the interface of F_1, if the entrance angle θ is larger than the critical angle θ_c, the beam will experience a Goos-Hänchen shift d_g [25] that is a length about a wavelength of the pump light λ_p, and then is totally reflected into the fibre by the interface. In the distance of d_g, the pump beam tunnels the fibre out a distance of d_p that is also a length of λ_p, and then an evanescent field of the pump beam E_p is formed outside F_1. E_p is a traveling wave along the z-axis, but it can not travel along the x-axis [25], therefore, there is no electric field of E_p existing in the z-axis and this characteristic is independent on the polarization of the pump beam. For the evanescent-wave pumped laser, since no electric field of E_p exists in the z-axis, it is impossible to produce stimulated photons polarizing in the direction of z-axis. After dye gain is coupled into F_1, the WGM lasing oscillation and emission, of course, will lack the polarization element of z-axis, so the lasing radiation belongs to TE wave, of which electric field is strictly vertical to the axis of F_1.

WGM within a circular cavity is a kind of "Quasi-normal Mode" [26], meaning that part of energy in a WGM leaks tangentially out of the surface of the cavity in the way of evanescent-wave, which forms lasing emission in our situation as shown in the solid arrows of Fig.II-4-C. As both lasing emission and its electric vector are vertical to the axis of F_1,

based on a simple geometrical consideration, all electric vectors of lasing radiation that emit from the same big circle of F_1 , as shown in the dashed arrows of Fig.II-4-C, cross at the centre of the big circle. Therefore, when pump beam travels strictly along the axis of F_1, the lasing emission from evanescent-wave pumped WGM fibre laser is a special axial polarized emission of which emitting direction is vertical to the axis of F_1.

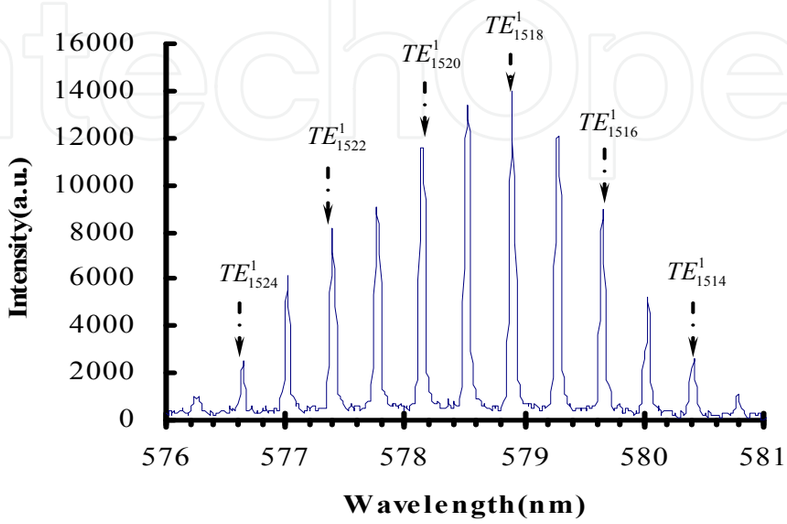

Fig. II-3. WGM lasing spectrum of TE wave acquired by pump beam being along a fibre's axis.

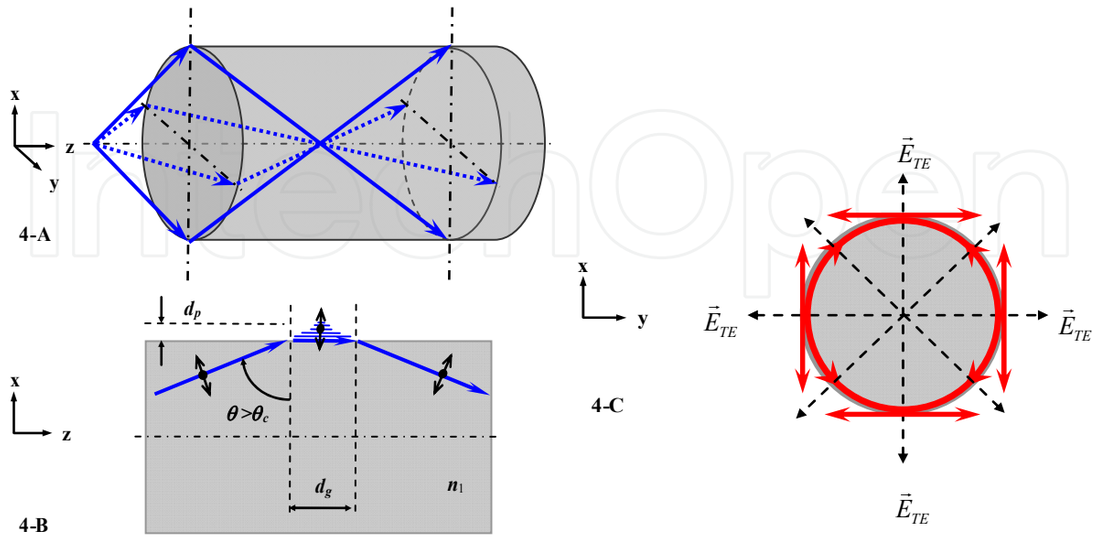

Fig. II-4. Diagram for the formation of radial polarization laser.

3.2.3 Pump deviating from the optical fibre's axis

When pump beams deviate from the axial direction of F_1, the lasing spectrum acquired by removing out the polarizer P_3 is shown in Fig.II-5-A. The spectrum is consisted of a group of weaker spectral lines and a group of stronger spectral lines, and each group is of the same wavelength interval. The lasing spectrum got by adding P_3 in the direction of y-axis is shown in Fig.II-5-B. The group of weaker lines vanishes completely in the spectrum, and the TE-wave spectrum remains. The lasing spectrum obtained by adding P_3 in the direction of z-axis is shown in Fig.II-5-C. The group of stronger lines almost vanishes in the spectrum, and the TM-wave spectrum remains. Fig.II-5 indicates that, when pump beam deviates from the fibre F_1's axis, both TE and TM waves exist in the lasing emission.

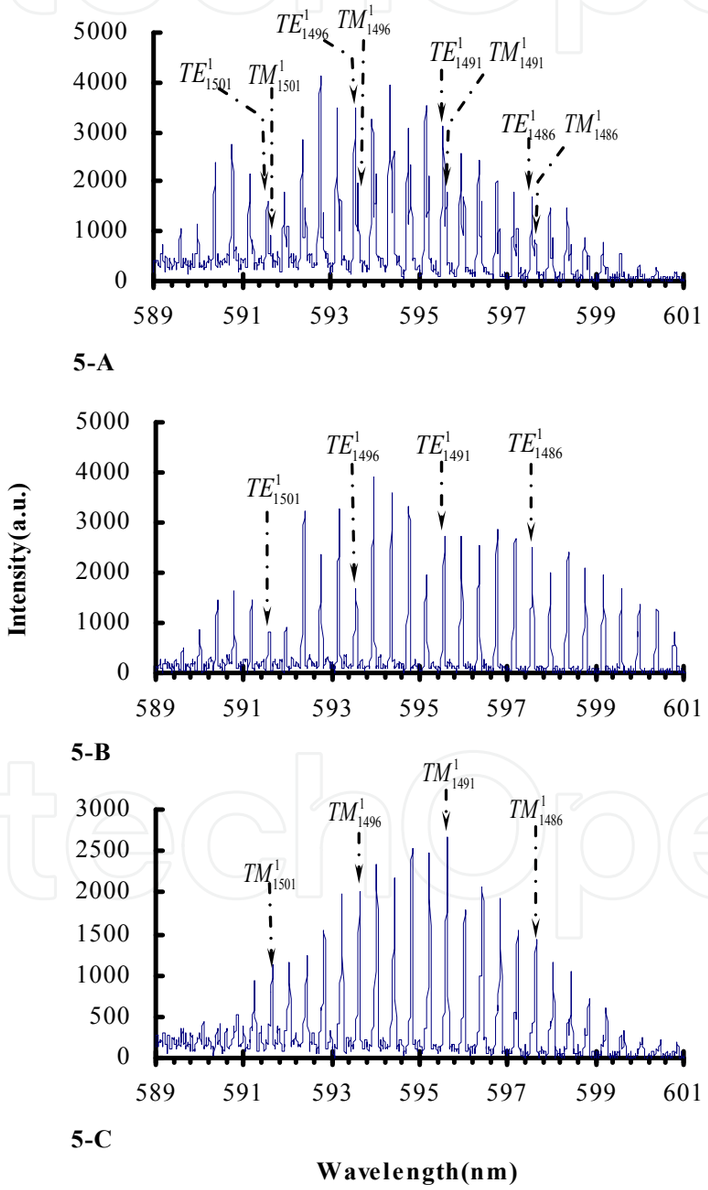

Fig. II-5. WGM lasing spectrum of TE& TM mixed wave acquired by pump beam deviating from the optical fibre's axis laser by paraxial pumped.

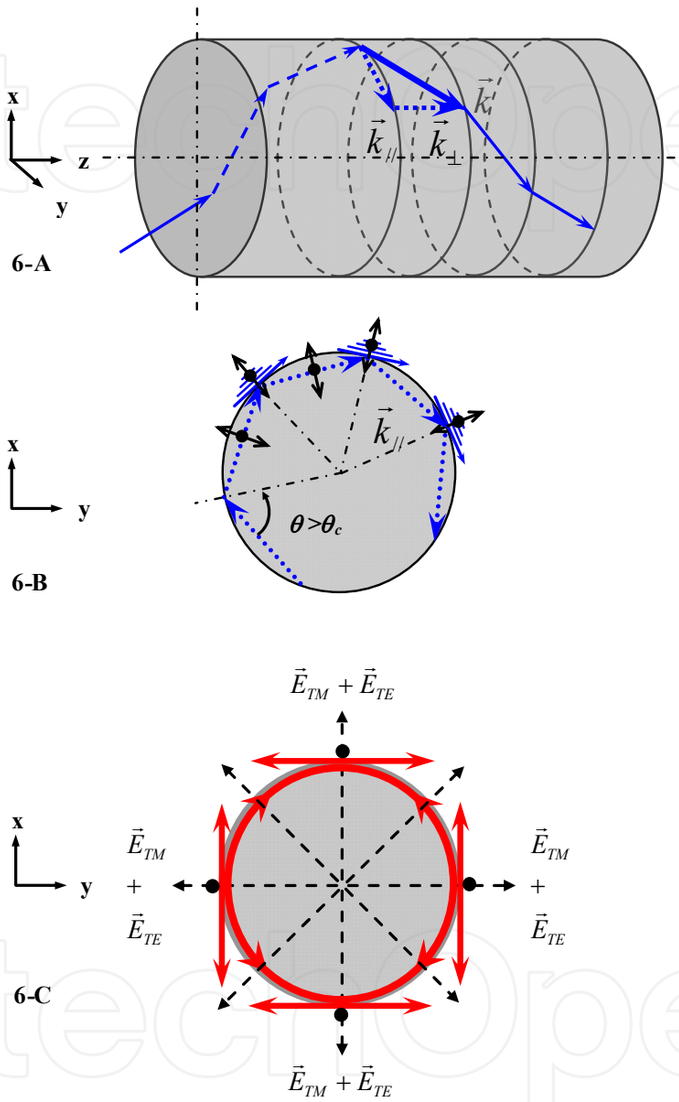

Fig. II-6. Diagram for the formation of mixed polarization laser.

3.2.4 The form of radial and axial mixing polarization laser

When pump beams are deviated from the optical fibre's axis, as shown in Fig.II- 6-A, the beams propagate as skew beams in the fibre F_1 along the z-axis. To analyse the property of the beams in the fibre, one of the beams with wave vector $\vec{k}$ is taken as an analytic sample. The vector $\vec{k}$ can be decomposed into $\vec{k}_{//}$ and $\vec{k}_{\perp}$, as shown in Fig.II-6-B in dashed arrow,

$\vec{k}_{//}$ is a component that expresses a light beam propagating in the xy plane by TIR; while $\vec{k}_{\perp}$ is a component that expresses a light beam propagating along the z-axis. For the beam expressed by $\vec{k}_{//}$, both electric vectors, the vector being parallel to z-axis and the vector being vertical to z-axis, exist simultaneously in the fibre F_1, when the beam experiences TIR on the fibre's interface, as shown in Fig.II-6-B, both electric vectors also exist in the evanescent field of pump beam. Because the dye molecules in the evanescent field of pump beam are excited by two different electric vectors, two kinds of stimulated photons, polarizing in the z-axis and in the xy plane, therefore, exist simultaneously in the evanescent field of WGMs of the circular cavity built in the optical fibre F_1. After the dye gain is coupled into the circular cavity, the WGM lasing oscillation and emission, of course, contain TE wave that is polarizing in the xy plane and TM wave that is polarizing along the z-axis. Combining with the analysis at the end part of this text 2.2, as shown in Fig.II-6-C, it can be conluded that the electric field of TE wave crosses at the centre of the circular cavity, while the electric field of TM wave is parallel to the z-axis; when pump beams are deviated from the axis of the optical fibre, the lasing emission from evanescent-wave pumped WGM fibre laser is a mixed polarization emission.

4. Part III - Linearly polarized three-color lasing emission from an evanescent wave pumped and gain coupled fibre laser

In Part III, an evanescent-wave pumped and gain coupled WGM fiber laser is introduced by inserting a bare quartz fiber (no cladding layer) into a glass capillary filled with dye molecules in a lower refractive index solution. Once the bare fiber is inserted into three glass capillaries filled with Rhodamine 6G, Rhodamine 610 and Rhodamine 640 dye solutions, respectively, WGM laser oscillations at the wavelengths of 567-575, 605-614 and 656-666 nm occur simultaneously, and a linearly polarized three-color lasing emission is achieved in a single optical fiber.

4.1 Experimental setup

The experimental setup is shown in Fig.I-4 schematically. An bare fiber (F_1, 196±1 μm in diameter, refractive index 1.458) was inserted into a long glass capillary (C, 1 mm in inner diameter), the residual space between F_1 and C was filled with ethanol and ethylene-glycol mixed solution doped by Rhodamine 6G dye with a concentration of 3×10^{-3} M/L. The refractive index of the mixed solution, acting as the cladding solution of F_1, was 1.395 measured by an Abbe refractometer. The pump beam was longitudinally coupled into F_1 along the fiber's axis by a lens (L) (focal length =75 mm) with a conical angle of θ_i =9.2°. The beam would propagate within F_1 by TIR if the conical angle θ_i was smaller than the critical entrance angle θ_{ic}, which was 35.6° in our experiments.

The evanescent field of the pump light (E_p) excites dye molecules in the mixed solution, thus the photons in evanescent field of WGM (E_{WGM}) of a circular cavity stimulate the excited dye molecules, and the E_{WGM} also couples dye gain into the circular cavity at the same time. Supported by the WGMs, lasing oscillations occur in the circular cavity. The WGM lasing emission (L_{WGM}) from the rim of F_1 can be recorded by a spectrometer (Spectrapro 500i) equipped with an ICCD detector (PI-Max 1024RB) via an optical fiber F_2, it gives 0.05 nm spectral resolution when a grating of density 2400g/mm is used. The intensity of L_{WGM} is

detected by a photo detector (PD, DSi200) after the lasing emission passing through an analyzer P_3 positioned on the *yz* plane.

4.2 Experimental results and discussion

4.2.1 Three-color WGM lasing emission

It is found that the generating length of lasing emission along the F_1 increases with pumping energy by arranging pump configuration as described in the part I, in which the fiber F_1 was replaced by a thick fiber (288 μm in diameter) and the direction of the incident beam was still strictly along the axial direction of F_1. When the pumping energy equaled 20, 50 and 100 μJ/pulse, the lengths of the lasing emission were 40, 90 mm and over 120 mm, respectively. Based on this, a longer gain length in evanescent-wave pumped WGM fiber laser, of course, can be utilized to build a multicolor WGM fiber laser [27]. That is to say, the fiber F_1 was inserted into three short glass capillaries (15 mm long) in series and their intervals between the capillaries were 5 mm. Rhodamine 6G, Rhodamine 610 and Rhodamine 640 dye molecules were dissolved in ethanol and ethylene-glycol mixed solution to obtain concentrations 5×10^{-4}, 2×10^{-3} and 1×10^{-2} M/L, respectively. The prepared dye solutions with an index of 1.422 were filled in the residual space between the F_1 and the capillaries. Evanescently pumped by 532 nm line of the pulsed YAG laser along the fiber's axis, only a weak fluorescent light emitted out from the fiber when the pumping energy was 20 μJ/pulse. The fluorescent spectrum was recorded by a spectrometer with a grating of density 150g/mm, which is the grey curve shown in Fig. III-1A. When pumping energy was 80 μJ/pulse, we observed three-color (yellow, orange and red) WGM lasing emissions simultaneously in experiments, the emitting wavelengths from the fiber laser were in the ranges of 567-575 nm (Rhodamine 6G), 605-614 nm (Rhodamine 610) and 656-666 nm (Rhodamine 640) as shown in Fig. III-1A with the black curve. Since three-color WGM lasing emission from a single optical fiber was realized, a novel evanescent-wave pumped and gain coupled WGM fiber multicolor laser was demonstrated eventually.

To show the fine spectral structure of the three-color WGM lasing emission, the spectra were recorded with a grating of density 2400g/mm, and shown in Figs. III-1B, 1C, and 1D in the wavelengths 567-575 nm, 605-614 nm and 656-666 nm, respectively. The measured spectral intervals between two adjacent peaks are 0.246 nm (Fig.III-1B), 0.282 nm (Fig.III-1C) and 0.335 nm (Fig.III-1D), which can be compared with the calculated free spectral widths of WGMs in the used circular cavity. For a larger diameter fiber (288 μm in our case), the wavelength intervals (free spectral width) can be approximately calculated by [27] $\Delta\lambda = \lambda^2/2\pi an_1$, where a and n_1 are the radius and the refractive index of the used fiber, respectively. The calculated wavelength intervals are 0.247, 0.281 and 0.332 nm in the wavelength ranges of 567-575 nm, 605-614 nm and 656-666 nm, which accord well with the measured values.

4.2.2 Spacial overlap between evanescent wave of WGM and lasing gain

To explain the characteristic of the longer gain in an evanescent-wave pumped WGM fiber laser, the radial intensities of the WGMs in the used circular cavity and the evanescent field of pump light are calculated. For a TE wave in a cylindrical coordinate system shown in the top left of Fig.I-4, the electric field of a WGM in a cylindrical cavity can be written as (I-6c, 6d). For TM wave with radial mode number l and angular mode number n, the WGM is

assigned by TM_n^l (l, n), while it is assigned by TE_n^l (l, n) for TE wave in this part. Two lasing lines at the wavelengths of 591.59 and 589.43 nm have been mode assigned [20,28] as TE_{1500}^1 and TE_{1490}^2 , which are chosen to calculate the distribution of radial intensity. Let a = 98 μm, n_1 =1.458, and n_2 =1.395, the radial intensities $I_{WGM}(r)$ for the two WGMs are calculated and shown in Fig.III-2.

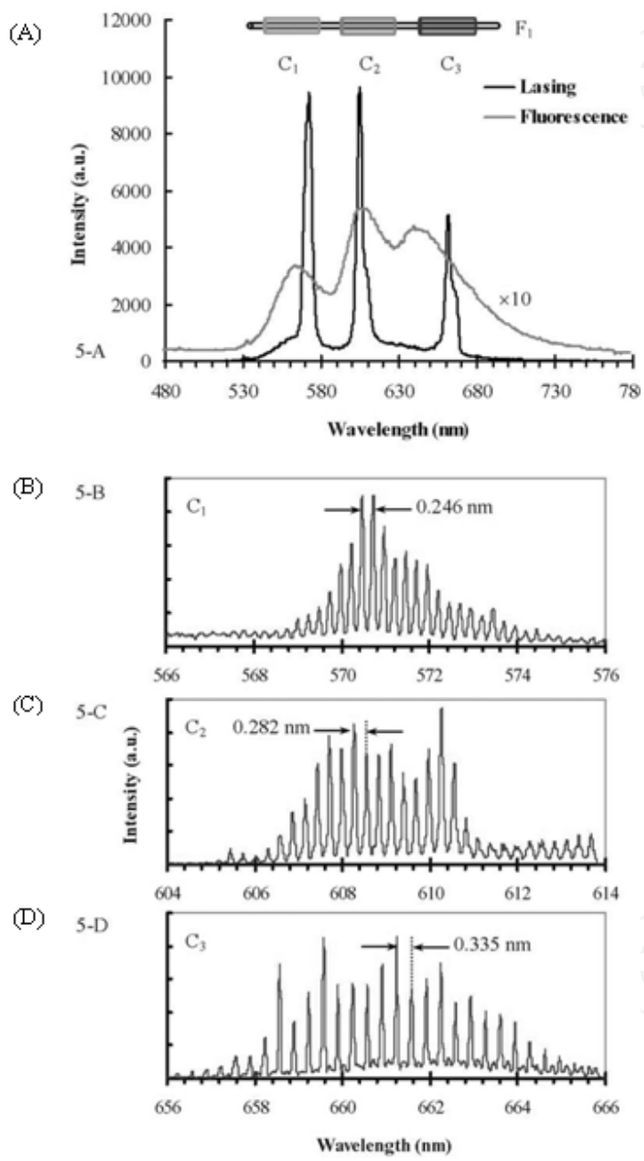

Fig. III-1. Lasing spectra recorded by gratings with densities: 150g/mm (A) and 2400g/mm (B), (C) and (D). Panel (A) shows fluorescent (grey curve) and lasing (black curve) spectra emitting from a three-colour evanescent-wave fiber laser, and the laser structure with the capillaries C_1, C_2 and C_3 being filled with different dye solutions. Panels (B), (C) and (D) indicate lasing spectra emitted from C_1, C_2 and C_3 filled with Rhodamine 6G, 610 and 640 dye solutions, respectively.

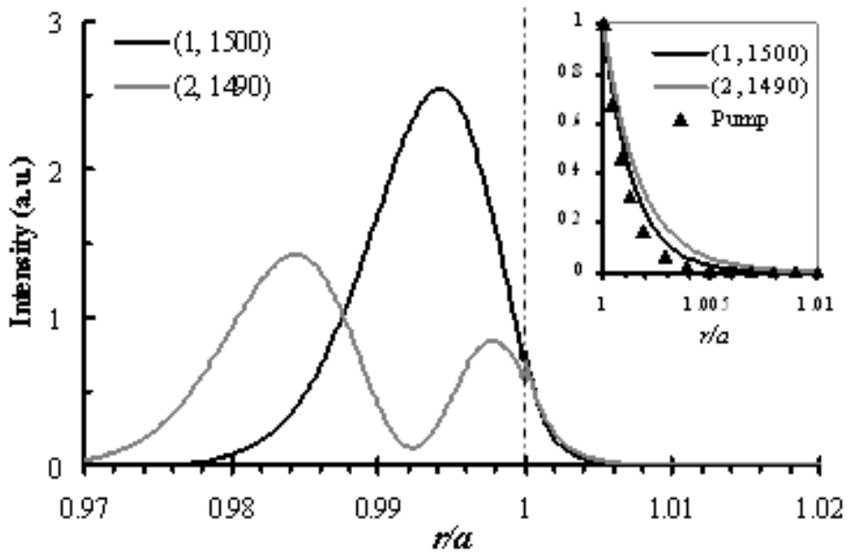

Fig. III-2. Radial intensity distributions calculated for two WGMs assigned by TE^{1}_{1500} (1, 1500) and TE^{2}_{1490} (2, 1490), where the bumps at $r = a$ are caused by the discontinuity of TE wave, and the insert shows the intensities of evanescent waves for the pump light (solid triangles) and WGMs (black and grey curves)

The evanescence-wave intensity of the pump light is also calculated from [16]

$$I_p(r) = I_0 \exp[-2k\beta(r/a - 1)a], \quad (r \geq a), \tag{III-1}$$

where $\beta = [n_1^2 \sin^2\theta / n_2^2 - 1]^{1/2}$, and $k = 2\pi n_2/\lambda_p$. Letting I_0=1, θ =86.8°, λ_p = 532 nm, the calculated result is shown in the insert of Fig. 6 by solid triangles, for a convenient comparison, the normalized evanescent-wave intensities of the modes TE^{1}_{1505} and TE^{2}_{1490} are also presented. The curves in the insert show clearly that in the radial direction of the cylindrical cavity ($r \geq a$), the intensity distributions of the two WGMs overlap well with the distribution of evanescence-wave of the pump light. Because the lasing gain in the evanescent-wave pumped WGM fiber laser is excited by the evanescent field of the pump light, the spatial distribution of the lasing gain is the same as that of the pump light. Therefore, it is reasonable to attribute the longer gain distance and the higher pumping efficiency in evanescent-wave pumped WGM fiber laser to the good spatial overlap between the lasing gain and the evanescent field of WGMs in a circular cavity.

5. Part IV - Broadening free spectral range of an evanescent-wave pumped Whispering-Gallery-Mode fibre laser by Vernier effect

In Part IV, evanescent-wave pumping scheme is used in a WGM fibre laser, which is formed by inserting a piece of bare quartz fibre (without cladding) into a glass capillary filled with a dye solution of low refractive index, as shown in Fig.IV-1*a*. When the pumping light propagates along the fibre's axis by total internal reflection, its evanescent-field excites a lasing gain around the fibre, and WGM lasing emission occurs as the pumping energy

exceeds the threshold. To increase the FSR of WGM fibre laser, two optical fibres of different radii are bound together with their axes parallel to make a coupled cylinder-cavity structure (CCCS). Due to the Vernier effect [29-31], lasing occurs only when both cavities are in resonance at the same frequency, and the FSR of the CCCS is thus greatly enlarged.

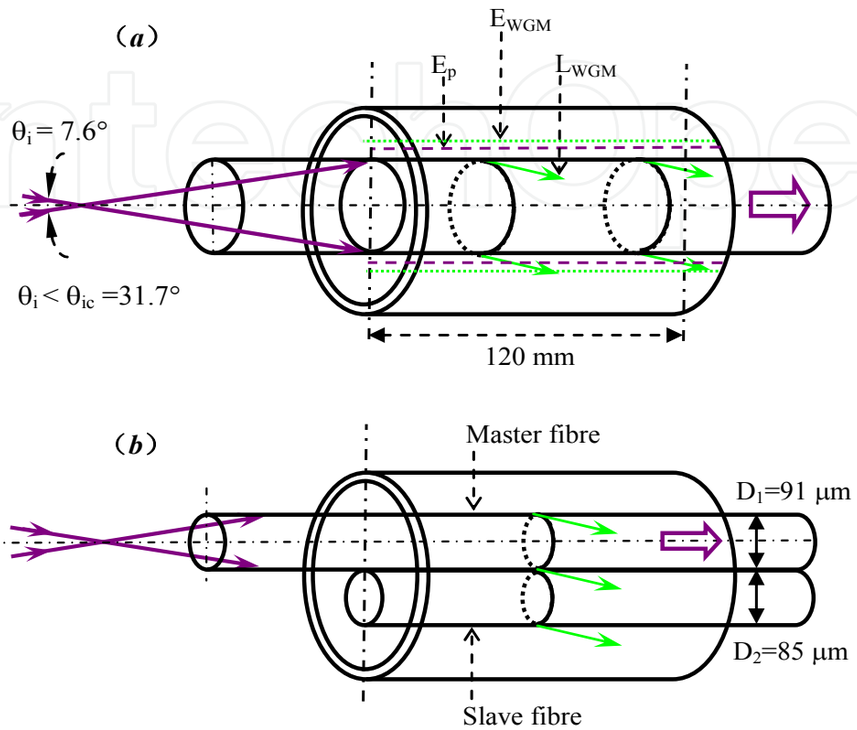

Fig. IV-1. Schematic of evanescent-wave pumped WGM fiber laser is shown in (*a*), where E_p and E_{WGM} indicate the evanescent-fields of the pump light and WGMs, L_{WGM} indicates the WGM lasing emission. The coupled cylinder-circular cavity is shown in (*b*), the master fiber provides the gain and make up a CCCS with the slave fibre. Note that the vertical and horizontal directions are drawn with different scales

5.1 Experiment and results

The experimental setup is shown in Fig.IV-1a. A laser beam (355 nm), generated by a frequency tripled and Q-switched Nd:YAG laser, was used as the pump light. A bare fibre (refractive index 1.46) was inserted into a long glass capillary (1 mm inner diameter), and the open space between the fibre and the capillary was filled with ethanol solution doped by Coumarin 500 (LC 5010, Lambda Physik) dye with a concentration of 4×10^{-3} Mol/L. The refractive index of the dye solution, acting as the cladding layer of the bare fibre, is 1.36 measured by an Abbe refractometer. The pump beam was coupled into the bare fibre along its axis with a conical angle θ_i =7.6°. The beam would propagate within the bare fibre by total internal reflection if the conical angle θ_i was smaller than the critical entrance angle θ_{ic}, that was 31.7° in our experiments. The evanescent field of the pump light (E_p) excites dye molecules in the dye solution, thus the photons in evanescent field of WGM (E_{WGM}) of a circular cavity (formed by any cross section of the fibre) stimulate the excited dye molecules, supported by the WGMs, lasing oscillations occur in the circular cavity. It is worth noting that the evanescent-wave pumping scheme used in this work is different from those of references

[30] and [31]. The ring cavity in reference [30] is composed by gain material and the gain is obtained by directly pumping the cavity, while the side-pumping scheme is used in reference [31]. The WGM lasing emission (L_{WGM}) from the rim of the fibre can be recorded via a detecting fibre by a spectrometer (Spectrapro 500i) equipped with a CCD detector (PI-Max 1024RB), which gives 0.05 nm spectral resolution when a grating of density 2400g/mm is used.

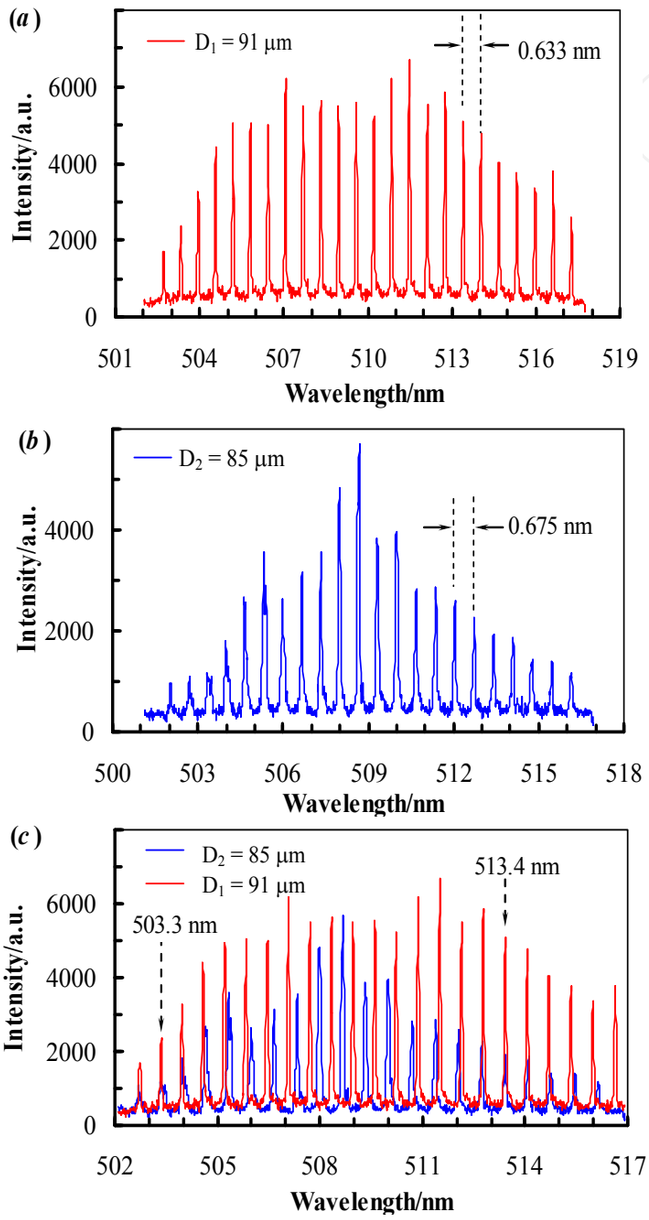

Fig. IV-2. WGM fiber lasing spectrum from a bare optical fibre of diameter D_1 = 91 μm is shown in (*a*), the measured FSR is 0.633 nm as indicated by the arrows. The spectrum from the bare optical fibre of diameter D_2 = 85 μm is shown in (*b*), the measured FSR is 0.675 nm as indicated by the arrows. The combination of spectra (*a*) and (*b*) in the same wavelength region is shown in (*c*). Two arrows in (*c*) indicate the overlapping positions of the WGM resonant wavelengths of the two fibers.

Two types of fibres with diameter D_1 = 91 μm and D_2 = 85 μm, measured by a microscope with 1 μm uncertainty, were prepared by etching two bare quartz fibres of original diameter 100 μm in a diluted HF-acid solution. After supersonic cleaning in ethanol, one of the fibres was inserted in the glass capillary filled with ethanol dye solution. The fibre was evanescently pumped by the 355 nm laser beam along its axis, and WGM lasing spectra were investigated. For the fibre with a diameter D_1 = 91 μm (D_2 = 85 μm), lasing emission was observed when the pumping energy was larger than 25 μJ (30 μJ), and the lasing spectrum was recorded as shown in Fig.IV-2a (Fig.IV- 2b) with the pumping energy fixed at 100 μJ. The measured average FSR in the spectral range from 504 to 516 nm was 0.633 nm for the fibre of D_1 = 91 μm, while it was 0.675 nm in the spectral range from 506 to 513 nm for the fibre of D_2 = 85 μm. When the two spectra (Fig.IV-2a and 2b) are merged together in the same wavelength region, as shown in Fig.IV-2c, it is found that two pairs of peaks corresponding to WGM resonant wavelengths overlap, and the overlapping wavelengths are 503.3 nm and 513.4 nm as indicated in Fig.IV-2c by the dashed arrows.

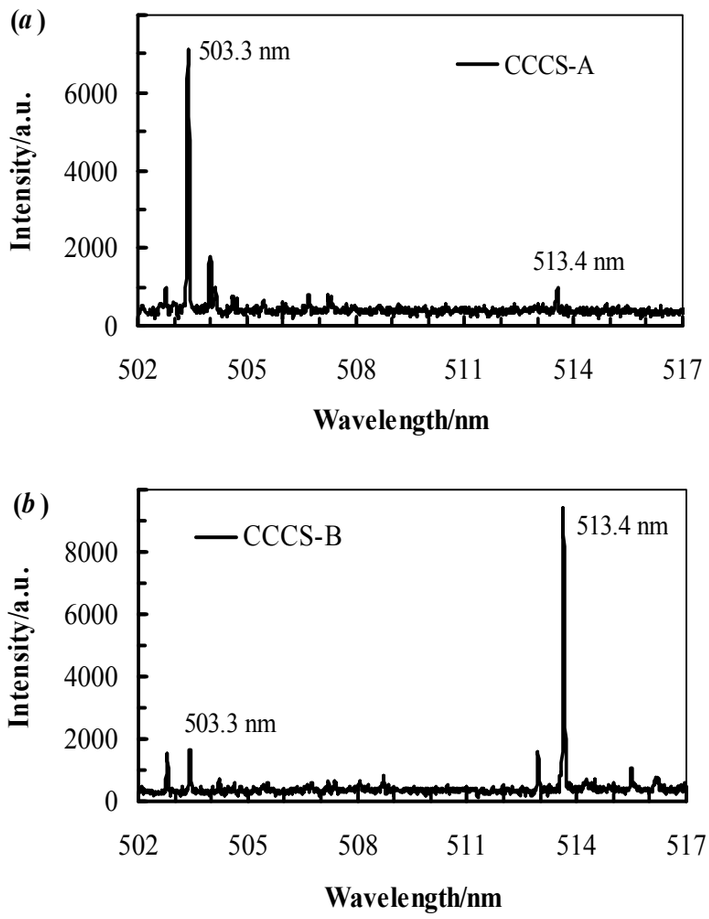

Fig. IV-3. Lasing spectra from the CCCS. The spectra (*a*) and (*b*) were acquired by setting a detecting fibre at different positions along the axis of the CCCS. The wavelength values shown in the figure are the same as the overlapping positions of the WGM resonant wavelengths in Fig.IV- 2(c).

After the single fibre experiments, the two fibres (we called the fibre of D = 91 μm in diameter as master fibre, and the fibre of D_2 = 85 μm in diameter as slave fibre) were bound together with their axes parallel by two fine hairs to form a CCCS. The CCCS was then inserted in the same glass capillary as shown in Fig.IV-1b, evanescently pumped by the 355 nm laser beam along the axis of the master fibre (pumping energy was fixed at 100 μJ), the lasing emissions were observed along the rims of both fibres, and the lasing spectra recorded were shown in Fig.IV-3. The CCCS suppresses most of WGM resonant peaks shown in Fig.IV-3. However, a strong lasing peak appears at 503.3 nm and a weak peak appears at 513.4 nm, where two pairs of peaks overlap together as shown in Fig.IV-2c. When the detecting fibre was moved to another position along the master fibre's axis, as shown in Fig.IV-3b, we obtained another lasing spectrum similar to that shown in Fig.IV-3a from the CCCS, in which most of WGM resonant peaks have been suppressed, such that a strong lasing peak appears at 513.4 nm and a weak peak appears at 503.3 nm. The wavelength difference between the strong and the weak peaks is 10.1 nm. This value, corresponding to FSR of the CCCS, is 16 and 15 times larger than that of the master and slave fibres, respectively. That is FSR is broadened by using the CCCS. The lasing peaks around 503.3 and 513.4 nm are possibly caused by the partial overlap of resonant frequencies between the WGMs of the main and the slave fibres.

5.2 Discussion and conclusion

Let D and m be the diameter and the refractive index of a circular cavity, respectively, the WGM resonant condition can be approximately written as $\pi Dm = N\lambda$, where λ is resonant wavelength, N is an integer. For the master and the slave fibres, the resonant conditions are given by,

$$\pi D_1 m = N_1 \lambda_1 , \tag{IV-1}$$

$$\pi D_2 m = N_2 \lambda_2 \tag{IV-2}$$

For a CCCS composed by two circular cavities, based on Vernier effect, the resonance occurs only at the same wavelength of both cavities satisfies resonant condition, which leads to $\pi(D_1 - D_2)m = (N_1 - N_2)\lambda_{CCCS}$, where λ_{CCCS} is the resonant wavelength of the CCCS. Therefore, the FSR of the CCCS can be written as,

$$FSR_{CCCS} = \delta\lambda_{CCCS} = \frac{\lambda_{CCCS}^2}{\pi(D_1 - D_2)m} . \tag{IV-3}$$

Instead of using the measured diameters of the two fibres, we utilize the spectral diameter defined by $D^s = \lambda^2 / \pi m \delta\lambda$ to calculate $\delta\lambda_{CCCS}$, where $\delta\lambda$ is the measured FSR from the lasing spectrum shown in Fig.IV- 2. For the master and the slave fibres, the spectral diameters are D_1^s = 89.6 μm ($\delta\lambda$ = 0.633 nm) and D_2^s = 84.0 μm ($\delta\lambda$ = 0.675 nm), respectively. Substituting the values of D_1^s and D_2^s , together with m = 1.46 into equation (3), the calculated $\delta\lambda_{CCCS}$ is 10.28 nm for λ_{CCCS} = 513.4 nm, and 9.87 nm for λ_{CCCS} = 503.3 nm. The average value of $\delta\lambda_{CCCS}$ is 10.08 nm, which is very close to the measured FSR of the CCCS.

A broad FSR can also be obtained by using a single fibre of small diameter. For example, the diameter must be reduced to about 6 μm to obtain the same FSR as the CCCS used in this work. However, a fibre of small diameter means a low efficiency to couple the pumping energy into the fibre, as well as a decrease in its quality factor due to a larger leakage loss, especially when the cavity is immersed in a liquid solution.

The difference between the geometric diameters (D_1 = 91 μm, D_2 = 85 μm) and the spectral diameters (D_1^s = 89.6 μm, D_2^s = 84.0 μm) is mainly caused by the property of intensity distribution of WGMs. Most of photons in a WGM don't travel strictly along the inner surface of a circular cavity, but slightly inside the surface. Therefore, the spectral diameter (D_i^s) calculated by the measured FSR of a circular cavity is always smaller than its geometric diameter (D_i).

6. Chapter summary

Threshold property of the novel WGM fiber lasers pumped by an evanescent-wave has been investigated . The laser has been fabricated by inserting a bare fused quartz fiber into a glass capillary filled with dye solution, and its energy threshold properties, including the energy threshold varied with the RI of the dye solution for different fiber diameters and the produced length of lasing emission, are experimentally studied. We find that the energy threshold is very sensitive to the change of the refractive index of dye solutions and the fiber diameter, and the produced length of lasing emission is dependent on dye concentration and the refractive index of dye solutions. Based on the characteristic of evanescent-wave pumping scheme, we derive the threshold energy formula of the WGM fiber lasers from the general theory of WGM microcavity laser. Based on the characteristic of frustrated totally internal reflection of light traveling along the fiber, we obtain the equation. to determine the produced length of lasing emission according to the characteristic of FITR of light traveling along the fiber. The calculated results with our theory fit the experimental data very well.

The polarization property of lasing emission, for the evanescent-wave pumped WGM fibre laser, is related closely to the light-pump conditions. When pump beams travel strictly along the axis of the optical fibre, only TE wave exists in lasing emission, and the electric vector of the lasing emission goes along the radial direction of the fibre, which forms a special radial polarization emission whose emitting direction is vertical to the fibre's axis. When pump beams are deviated from the axis of the optical fibre, both TE and TM waves exist in lasing emission, which forms a special emission mixed with radial and axial polarization emission, and the emitting direction is also vertical to the fibre's axis.

For an evanescent-wave pumped and gain coupled WGM fiber laser, the dye gain is excited by the evanescent wave of the pumped light, distributed around the fiber and coupled into WGMs of a circular cavity. A good spatial overlap between the dye gain and the evanescent fields of WGMs leads to a high pumping efficiency and a longer gain distance along the fiber, and linearly polarized three-color lasing emissions from a single optical fiber can be realized by immersing the fiber into three different dye solutions, where may be found a potential application in multicolor display.

Evanescent-wave pumping scheme has been successfully used to excite WGM fibre laser. A coupled cylinder-cavity structure has been fabricated by binding two bare optical fibres

together, and the measured FSR of the laser emission from the CCCS is effectively broadened. This structure can be used to obtain a single mode lasing emission in an evanescent-wave pumped WGM fibre laser.

7. Acknowledgments

We acknowledge support from the National Science Foundation of China (NSFC) through grant 60877037、11164033 and the program of IRTSTYN in University of Yunnan Province.

8. References

[1] H. J. Moon, Y .T. Choung, and K. An, "Cylindrical micro-cavity laser based on the evanescent-wave-coupled Gain,"Phys. Rev. Lett. 85, 3161-3164 (2000).

[2] M .Kazes, D. Y. Lewis, Y. Ebenstein, T. Mokari and U. Banin, "Lasing from semicon ductor quantum roads in a cylindrical micro-cavity," Adv. Mater. 14, 317-321 (2002).

[3] H. J. Moon, G. W. Park, S. B .Lee, K. An, and J. H. Lee, "Waveguide mode lasing via evanescent-wave-coupled gain from a thin cylindrical shell resonator," Appl. Phys. Lett. 84 4547-4550(2004).

[4] N. K. Chen, L. Y. Zhang, K. C. Hsu, L. L. Hu, S .Chi, Y. C. Lai, S .M .Tseng, and J .T. Shy，"CW-pumped evanescent amplification based on side-polished fiber with heavily Er3+-doped glass overlay," Jpn. J. Appl. Phys . 45, 6328-6330 (2006).

[5] J. D. Suter, W. Lee, D. J. Howard, E. Hoppmann, I. M. White, and X. Fan, "Demonstration of the coupling of optofluidic ring resonator lasers with liquid waveguides," Opt. Lett. 35, 2997-2999(2010).

[6] X. Y. Pu, N. Jiang, D. Y. Han, Y. L. Feng, and Y. T. Ren, "Linearly polarized three-colour lasing emission from an evanescent wave pumped and gain coupled fibre laser," Chin. Phys. B 90, 054207_1-054207_7(2010).

[7] H. Fujiwarra, and K. Sasaki, "Lasing of a microsphere in dye solution," Jpn. J. Appl. Phys. 28, 5101-5104(1999).

[8] S. B. Lee, M. K. Oh, J. H. Lee, and K. An, "Single radial-mode lasing in a submicron-thickness spherical shell microlaser," Appl. Phys. Lett. 90, 201102_1-201102_4 (2007).

[9] A. Shevchenko, K. Lindfors, S. C. Buchter, and M. Kaivola, "Evanescent wave pumped cylindrical micro-cavity laser with intense output radiation," Opt. Commun. 245, 349-353(2005).

[10] S. Lacey, I. M. White, Y. Sun, S. I. Shopova, J. M. Cupps, P. Zhang, and X. Fan, "Versatile opto-fluidic ring resonator lasers with ultra-low threshold," Opt. Express 15, 15523-15530 (2007).

[11] X. Jiang, Q. Song, L. Xu, J. Fu, and L. Tong, "Microfibre knot dye laser based on the evanescent-wave-coupled Gain," Appl. Phys. Lett. 90, 233501_1-233501_3 (2007).

[12] C. Monat, P. Domachuk, and B. J. Eggleton, "Integrated optofluidics: A new river of light," Nat. Photonics 1, 106-114(2007).

[13] Y. Sun, S. I. Shopovab, C. S. Wu, S. Arnold, and X. Fan, "Bioinspired optofluidic FRET lasers via DNA scaffolds," PNAS 37, 16039-16042(2010).

[14] X .Y. Pu, N. Jiang, R. Bai, W. L . Xiang，Y. X. Zhang, and D. Y. Han, "A novel micro-cavity fiber laser with three-colorWGM lasing emission in a single optical fiber," Chinese Patent No.ZL200810058304 (30 Sep. 2009).

[15] K. M. Djafar, and L. S. Lowell, *Fibre-optic Communications Technology*(Science Press, Beijing, 106-108(2002)).

[16] M. Born, and E. Wolf, *Principles of Optics*(Cambridge University Press, Cambridge, 1997).

[17] C. F. Bohren, and D. R. Huffman, *Absorption and Scattering of Light by Small Particles*(John Wiley & Sons,New York, 1998).

[18]Y. X. Zhang, X.Y. Pu, K. Zhu, and L. Feng, "Threshold property of Whispering- Gallery-Mode fiber lasers pumped by evanescent-wave," J. Opt. Soc. of Am. B. 28, 2048-2056 (2011)

[19] Y. S. Choi, H. J. Moon, K. Y. An, S. B. Lee, J .H. Lee, and J. S. Chang, "Ultrahigh-Q Microsphere Dye Laser Based on Evanescent-Wave Coupling," J. Korean Phys Soc. 39, 928-931(2001).

[20] C. C .Lam, P. Y .Leung, and K. Yang , "Explicit asymptotic formulas for the positions, widths, and strengths of resonances in Mie scattering," J. Opt. Soc. of Am. B. 9, 1585-1592(1992).

[21] D. L. Wang, N. Jiang, L. Q. Jiang, and X. Y. Pu, "The precise assignment of whispering gallery modes for lasing spectra emitting from cylindrical micro-cavities (in Chinese)," Spectroscopy Spectr Anal.28, 2749-2753(2008).

[22] D. G. Hall, "Vector-beam solutions of Maxwell's wave quation," Opt. Lett. 21, 9-11 (1996).

[23] Q. Zhan, J. R. Leger, "Microellipsometer with radial symmetry," Appl. Opt. 41, 4630-4637(2002).

[24] P. W. Barber, S. C. Hill, *Light scattering by particles: computational methods*. (World Scientific Publishing Co Pte Ltd, Singapore, 25-77(1990)).

[25] J. D. Jackson, *Classical Electrodynamics*. (Advanced Education Press, Beijing, 306-308 (2001)).

[26] E. S. C. Ching, P. T. Leung, K. Young, *The role of Quasi-normal Modes-Optical Processes in Microcavities*, edited by R. K. Chang and A. J. Campillo. (World Scientific Publishing Co Pte Ltd, Singapore, 1-75(1996)).

[27] X. Y. Pu, R. Bai, W. L. Xiang, F. Du and N. Jiang，"Two-wavelength-range whispering-gallery-mode fiber laser pumped by evanescent wave，" Acta Phys. Sin. 58, 3923-3928(2009).

[28] R. Yang, W. H. Yu, Y. Bao, Y. X. Zhang and X. Y. Pu, "whispering-gallery modes based on evanescent field in cylindrical micro-cavity," Acta Phys. Sin. 57, 6414-6418 (2008).

[29] K. Oda, N. Takato, and H. Toba, "A wide-FSR waveguide double-ring resonator for optical FDM transmission systems," IEEEJ. Light wave Technol. 9, 728-736 (1991).

[30] L. Shang, L. Liu, and L. Xu, "Single-frequency coupled asymmetric microcavity laser,"Opt. Lett. 33, 1150-1152 (2008).

[31] X. Wu, Y. Z. Sun, J. D. Suter, and X. D. Fan, "Single mode coupled optofluidic ring resonator dye lasers," Appl. Phys. Lett. 94 241109_1-241109_3 (2009).

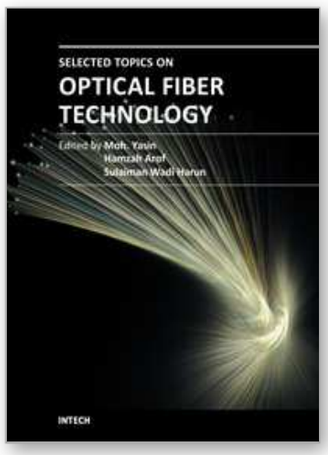

Selected Topics on Optical Fiber Technology

Edited by Dr Moh. Yasin

ISBN 978-953-51-0091-1

Hard cover, 668 pages

Publisher InTech

Published online 22, February, 2012

Published in print edition February, 2012

This book presents a comprehensive account of the recent advances and research in optical fiber technology. It covers a broad spectrum of topics in special areas of optical fiber technology. The book highlights the development of fiber lasers, optical fiber applications in medical, imaging, spectroscopy and measurement, new optical fibers and sensors. This is an essential reference for researchers working in optical fiber researches and for industrial users who need to be aware of current developments in fiber lasers, sensors and other optical fiber applications.

How to reference

In order to correctly reference this scholarly work, feel free to copy and paste the following:

Xiao-Yun Pu, Yuan-Xian Zhang and Li Feng (2012). Evanescent-Wave Pumped and Gain Coupled Whispering-Gallery-Mode Fibre Laser, Selected Topics on Optical Fiber Technology, Dr Moh. Yasin (Ed.), ISBN: 978-953-51-0091-1, InTech, Available from: http://www.intechopen.com/books/selected-topics-on-optical-fiber-technology/evanescent-wave-pumped-and-gain-coupled-whispering-gallery-mode-fibre-laser

INTECH
open science | open minds

InTech Europe
University Campus STeP Ri
Slavka Krautzeka 83/A
51000 Rijeka, Croatia
Phone: +385 (51) 770 447
Fax: +385 (51) 686 166
www.intechopen.com

InTech China
Unit 405, Office Block, Hotel Equatorial Shanghai
No.65, Yan An Road (West), Shanghai, 200040, China
中国上海市延安西路65号上海国际贵都大饭店办公楼405单元
Phone: +86-21-62489820
Fax: +86-21-62489821

IntechOpen